Semi-Annual Status Report on NASA Grant NAG1-616,

"An Experimental Investigation of
Dynamic Ground Effect"

September 19, 1985 - March 15, 1986

CRINC-FRL-717-1

by

Pai Hung Lee, C. Edward Lan, and

Vincent U. Muirhead

April 1, 1986

The Flight Research Laboratory

Department of Aerospace Engineering

The University of Kansas

Lawrence, Kansas 66045

TABLE OF CONTENTS

Page

LIST OF FIGURES.....ii

1. INTRODUCTION.....1

2. TEST FACILITY AND MODELS.....2

3. PRELIMINARY DATA ANALYSIS.....3

3.1 60-Degree Delta Wing.....3

3.2 F-106.....3

3.3 XB-70-1 Configuration.....5

4. REFERENCES.....7

LIST OF FIGURES

Page

Figure 1: Model Geometry of a 60-Degree Delta Wing.....9

Figure 2: Model Geometry of an F-106 Model.....10

Figure 3: Model Geometry of an XB-70-1 Model.....11

Figure 4: Sting Support and Strain Gage Arrangement.....12

Figure 5: Test Section with Model Support and Ground Board in the KU Wind Tunnel.....13

Figure 6: Longitudinal Aerodynamic Characteristics for 60-Degree Delta Wing in Out-of-Ground Effect.....14-15

Figure 7: Longitudinal Aerodynamic Characteristics for an F-106 Model in Out-of-Ground Effect.....16-18

Figure 8: Longitudinal Aerodynamic Characteristics for an F-106 Model in Static Ground Effect. H/b = 0.4.....19-21

Figure 9: Longitudinal Aerodynamic Characteristics for an F-106 Model in Out-of-Ground Effect with Flap Deflections.....22-24

Figure 10: Longitudinal Aerodynamic Characteristics for an F-106 Model with Flap Deflections in Static Ground Effect. H/b = 0.4.....25-27

Figure 11: Longitudinal Aerodynamic Characteristics for an F-106 Model with Flap Deflections in Static Ground Effect at Different Ground Heights. α = 14 Degrees.....28-30

Figure 12: Incremental Lift and Drag for an F-106 Model with Flap Deflections in Static Ground Effect at α = 14 Degrees.....31-32

Figure 13: Comparison of Some Static Ground Effect Data for the XB-70-1 Configuration from the KU and Langley 7 x 10 Tunnels.....33-35

Figure 14: Longitudinal Aerodynamic Characteristics for an XB-70-1 Model with Wing Alone in Static Ground Effect.....36-38

LIST OF FIGURES, continued

Page

Figure 15: Longitudinal Aerodynamic Characteristics for an XB-70-1 Model (W + B + V) in Static Ground Effect.....39-41

Figure 16: Longitudinal Aerodynamic Characteristics for an XB-70-1 Model (W + B + V + C) in Static Ground Effect.....42-44

Figure 17: Longitudinal Aerodynamic Characteristics for an XB-70-1 Model (W + B = V + C) with Flap Deflections in Out-of-Ground Effect.....45-47

Figure 18: Longitudinal Aerodynamic Characteristics for an XB-70-1 Model (W + B + V + C) with Flap Deflections in Static Ground Effect. H/b = 0.4....48-50

Figure 19: Effect of Flap Deflections on Longitudinal Aerodynamic Characteristics for an XB-70-1 Model at α = 14 Degrees in Static Ground Effect.....51-53

Figure 20: Incremental Lift and Drag for an XB-70-1 Model with Flap Deflections in Static Ground Effect at α = 14 Degrees.....54-55

Figure 21: Comparison of Ground Effect Data for the XB-70-1 Configuration from Flight Test and Wind-Tunnel Static Test at $\alpha \approx 9.5$ Degrees.....56

1. INTRODUCTION

In this report, some results in a wind tunnel testing program to investigate the ground effect associated with low-aspect-ratio aircraft during the landing takeoff operation will be presented. In this reporting period (September 16, 1985 - March 15, 1986) the main research activity was wing tunnel testing on two aircraft models and one delta wing model in a 3 x 4.3 foot low-speed wind tunnel at the University of Kansas.

The tasks in this reporting period were as follows:

1. Planning the test program
2. Checking the KU wind tunnel facility
3. F-106 model design and manufacture
4. F-106 static ground effect testing
5. Analysis of F-106 test data
6. 60-degree delta wing testing
7. Analysis of 60-degree delta wing test data
8. XB-70-1 model design and manufacture
9. XB-70-1 static ground effect testing
10. Analysis of XB-70-1 test data
11. Testing of a 60-degree delta wing in the Vortex Research Facility at Langley Research Center.

2. TEST FACILITY AND MODELS

These experimental studies were conducted to determine the longitudinal force and moment aerodynamic coefficients for a 1/48-scale model of an F-106 airplane and a 0.01-scale model of an XB-70-1 airplane. The two airplanes and one 60-degree delta wing models (see Figures 1, 2, and 3) were designed and fabricated to satisfy the specific test conditions of the KU wind tunnel with a 3 x 4.3 foot test section. The models were mounted at the front edge of the balance sting support (see Figure 4) which includes three strain gages to measure the lift, drag, and pitching moment of the airplane models. The static ground-effect tests were conducted in the wind tunnel by the ground-board methods (see Figure 5). Tests were made with a ground height varying from $H/b \approx 1.6$ to a low ground-board height, which depended on the model span length and the angle of attack. Before each run, the angle of attack was preset within a range from 0° to 34°. Based on the wing mean aerodynamic chord, the test Reynolds number was approximately 500,000 for the F-106 model and 750,000 for the XB-70-1 model. Several tests were made with the wing flap (elevon) deflection at 15° (trailing edge down) or -30° position. The strain gage signals sampled by the voltmeter were used along with the calibration factors by the Hewlett-Packard 9826 microcomputer to determine the lift, drag, and pitch moment coefficients.

3. PRELIMINARY DATA ANALYSIS

3.1 60-Degree Delta Wing

Lift data in Figure 6! show that the present results are consistent with Wentz's, except for $\alpha > 25$ degrees. However, the lift coefficients measured in the Langley Vortex Research Facility (VRF) tend to be lower and the drag coefficients tend to be higher as shown in Figure 6B. Exact reasons for the discrepancy are not known.

3.2. F-106

The longitudinal characteristics of a clean configuration of the F-106 out of ground effect are presented in Figures 7. The lift coefficients obtained in the Langley 12-foot tunnel are always lower than the present results (Figure 7A), although the vortex-breakdown characteristics appear to be quite similar. In addition, the drag coefficients are higher (Figure 7B) and the pitching moments are more positive (Figure 7C) from the 12-foot tunnel. For the latter, since the slopes of the moment curves for both sets of data are nearly the same, the discrepancy is not caused by the difference in the coordinates of moment center.

As expected, the wing-body lift is lower than that of the wing alone (Figure 7A) and the wing-body drag is higher (Figure 7B). Although the longitudinal stability of the wing-body configuration, as evidenced by the reduced moment-lift slope, is lower than that of

the wing alone, the zero-lift moment of the former is negative. This is probably caused by the nose camber of the fuselage.

The static ground effect on longitudinal aerodynamic characteristics is presented in Figures 8A-8C. As expected, the lift is increased and the drag is reduced in ground effect as shown in Figures 8A and 8B. Longitudinal stability tends to be increased substantially (Figure 8C).

Comparing the results with flap deflection in and out of ground effect (Figures 9 and 10) indicates that lift is increased as usual by ground effect. However, at a given C_L, D_D is not much different in ground effect (see Figures 9B and 10B) at low C_L. Again, the longitudinal stability is increased by ground effect (Figures 9C and 10C).

In Figure 11, variation of longitudinal characteristics with ground height is presented at an α of 14 degrees. With a positive flap angle of 15 degrees, lift increases more rapidly (Figure 11A); and the drag increase is much smaller (Figure 11B) as the ground height is reduced, when compared with a flap angle of -30 degrees. On the other hand, the pitching moment becomes much more negative with a positive flap angle as the ground board is approached.

Finally, the percent increases in lift and drag at $\alpha = 14$ degrees with ground height are presented in Figure 12. Although the lift increments for flap angles of ± 15 degrees and -30 degrees are approximately the same, the change in C_D is much lower with a positive flap angle, as it was indicated in Figure 11. This is

perhaps because with a positive flap angle, the leading-edge vortex flow is stronger and the conical camber of the F-106 will produce the effect of a vortex flap to reduce the drag.

3.3 XB-70-1 Configuration

The longitudinal characteristics of the XB-70-1 with various ground heights are presented in Figures 13. The lift coefficients obtained in the present (KU) datas are always higher than the Langley 7 x 10 foot results (Figure 13A). However, the lift-curve slope is seen to be in good agreement. In addition, the drag coefficients are higher (Figure 13B) and the pitching moments are more positive (Figure 13C) from the 7 x 10 foot tunnel. But the slopes of the moment curves for both sets of data are nearly the same.

The static ground effect on longitudinal aerodynamic characteristics of wing alone, wing-body-vertical-tail, and wing-body-vertical-tail-canard configurations are presented in Figures 14A-14C, Figures 15A-15C, and Figures 16A-16C, respectively. As expected, the lift is increased in ground effect (Figures 14A, 15A, and 16A) and the drag is reduced in ground effect at a given C_L (Figures 14B, 15B, and 16B). Meanwhile, the longitudinal stability tends to be increased substantially (Figures 14C, 15C, and 16C).

As expected, the lift and drag of the wing alone and wing-body configurations (Figures 14A, B; 15A, B; and 16A, B). However, the

canard tends to reduce the longitudinal stability greatly (Figures 14C, 15C, and 16C). Once the lift coefficient reaches 0.6 ($\alpha > 12°$), the pitch-moment slope relative to the quarter mean aerodynamic chord shows a trend from a negative to a positive value (Figure 16C). This variation of the pitch-moment slope indicates that the XB-70-1 has a longitudinal instability within the high angle-of-attack region.

Comparing the results with flap deflection in and out of ground effect (Figures 17 and 18) indicates that lift is increased as usual by ground effect at low C_L (Figures 17B and 18B). Again, the longitudinal stability is increased by ground effect (Figures 17C and 18C).

The longitudinal characteristics and the percent increases in ground effect are shown in Figure 19 and Figure 20, respectively. Variation with ground height is presented at an α of 14 degrees. The lift and drag are increased as the ground height is reduced (Figures 19A, 19B). The pitching moment becomes more negative as the ground board is approached (Figure 19C). In addition, the lift and drag percent increase at a flap angle of -30 degrees is higher than that at a flap angle of +15 degrees (Figures 20A, 20B).

Figure 21A compares flight and wing tunnel (static) ground-effect data at an angle of attack of about 9.5 degrees. The general trend for the increase in lift is the same for all three sets of data. However, there is considerable disparity in the magnitudes of the results.

REFERENCES

1. Pelagatti, C., Pilon, J. C., and Bardaud, J., "Analyse Critique des Comparaisons des Resultats de Vol aux Previsions de Soufflerie pour des Avions de Transport Subsonique et Supersonique," paper 23, AGARD CP-187, Flight/Ground Testing Facilities Correlation, 1975.

2. O'Leary, C. O., "Flight Measurements of Ground Effect on the Lift and Pitching Moment of a Large Transport Aircraft (Comet 3B) and Comparison with Wind Tunnel and Other Data," British ARC R&M 3611, June 1968.

3. Rolls, L. S., and Koenig, D. G., "Flight-Measured Ground Effect on a Low-Aspect-Ratio Ogee Wing Including a Comparison with Wind-Tunnel Results," NASA TND-3431, 1966.

4. Baker, P. A., Schweikhard, W. G., and Young, W. R., "Flight Evaluation of Ground Effect on Several Low-Aspect-Ratio Airplanes," NASA TND-6053, October 1970.

5. Chang, R. C., "An Experimental Investigation of Dynamic Ground Effect," KU-FRL-410-1, April 1985.

6. Fink, Marvin P., and Lastinger, James L., "Aerodynamic Characteristics of Low-Aspect-Ratio Wing in Close Proximity to the Ground," NASA Tech. Note D-926, 1962.

7. Wentz, William H., "Wind-Tunnel Investigations of Vortex Breakdown on Slender Sharp-Edge Wing," University of Kansas, 1968.

8. Pope, Alan, and Harper, John J., "Low Speed Wind-Tunnel Testing," John Wiley, Inc., 1965.

9. James C. Daugherty, "Wing-Tunnel/Flight Correlation Study of Aerodynamic Characteristics of a Large Flexible Supersonic Cruise Airplane (XB-70-1)," NASA TP-1514, 1979.

10. Lambourne, N. C., Bryer, D. W., and Maybrey, J. F. M., "The Behaviour of the Leading-Edge Vortices over a Delta Wing Following a Sudden Change of Incidence," British ARC R&M 3645, March 1969.

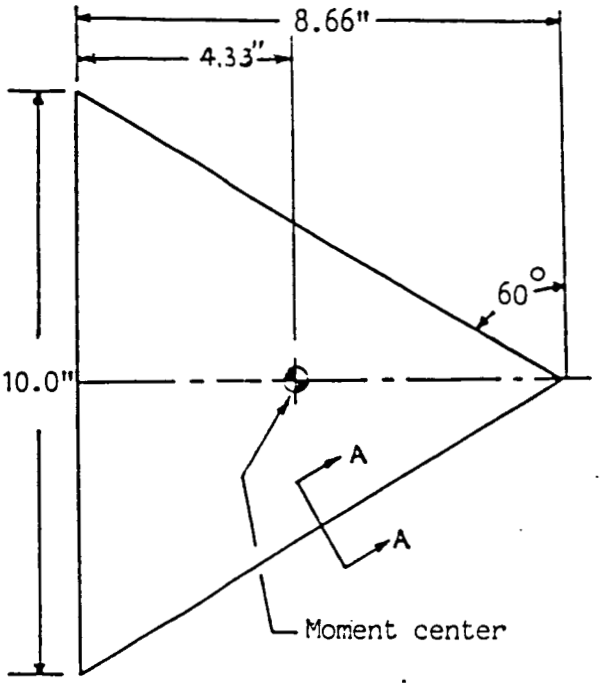

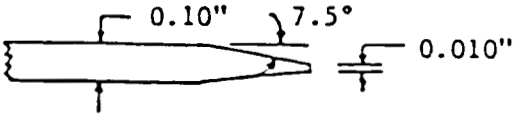

Section A-A (Enlarged)

Note: Section A-A is typical of all edges

Figure 1: Model Geometry of a 60-Degree Delta Wing

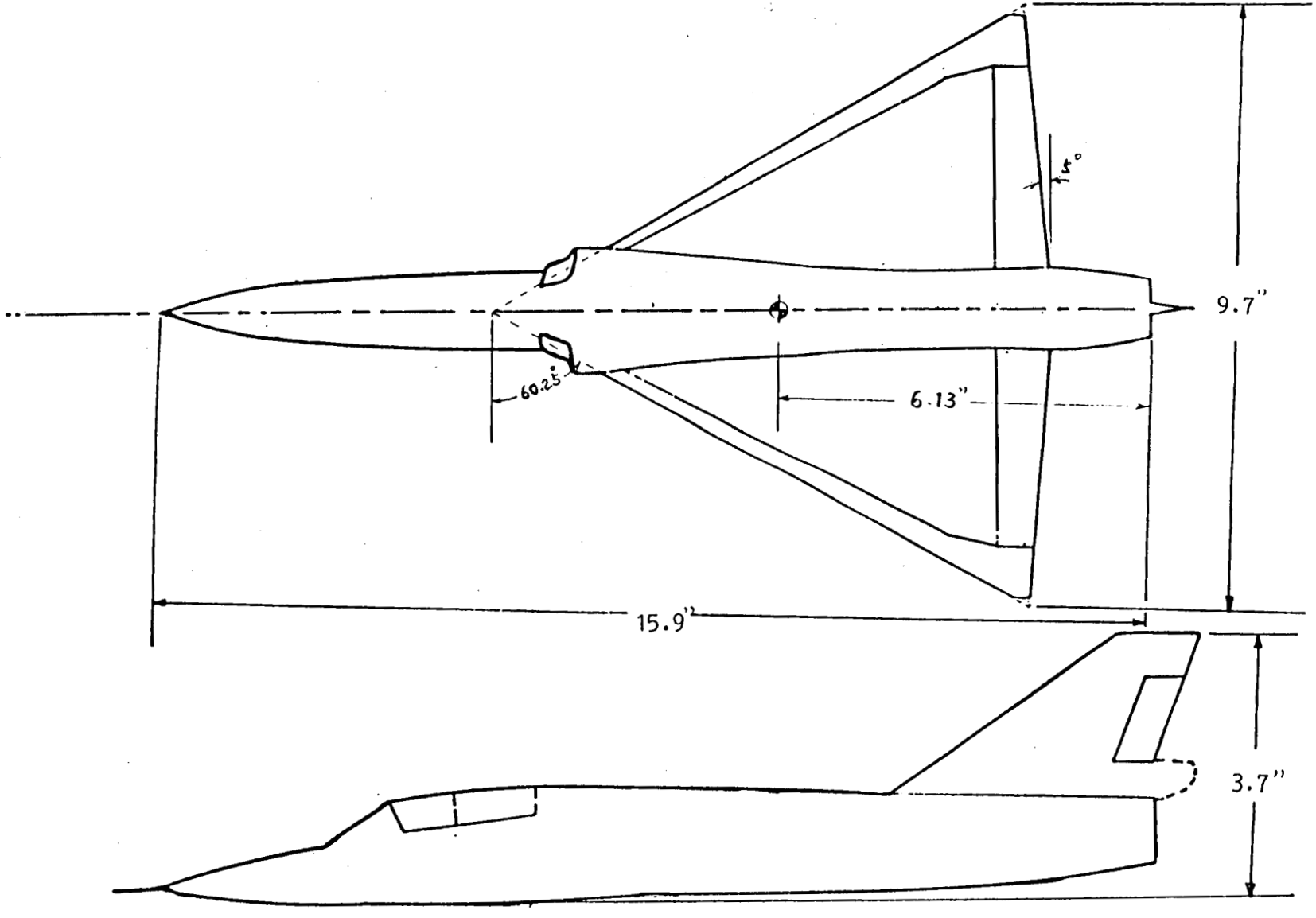

Figure 2: Model Geometry of an F-106 Model

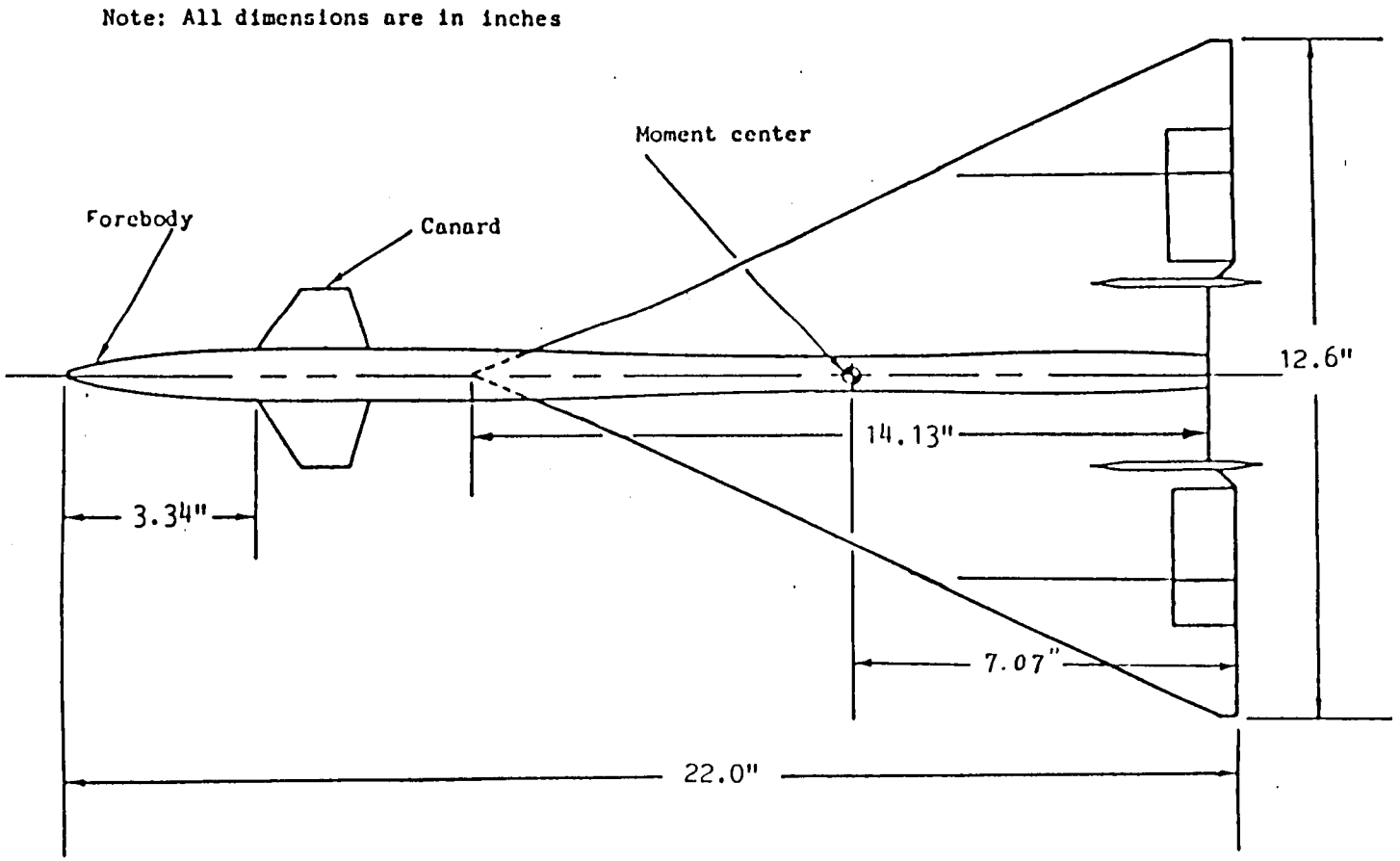

Figure 3: Model Geometry of an XB-70-1 Model

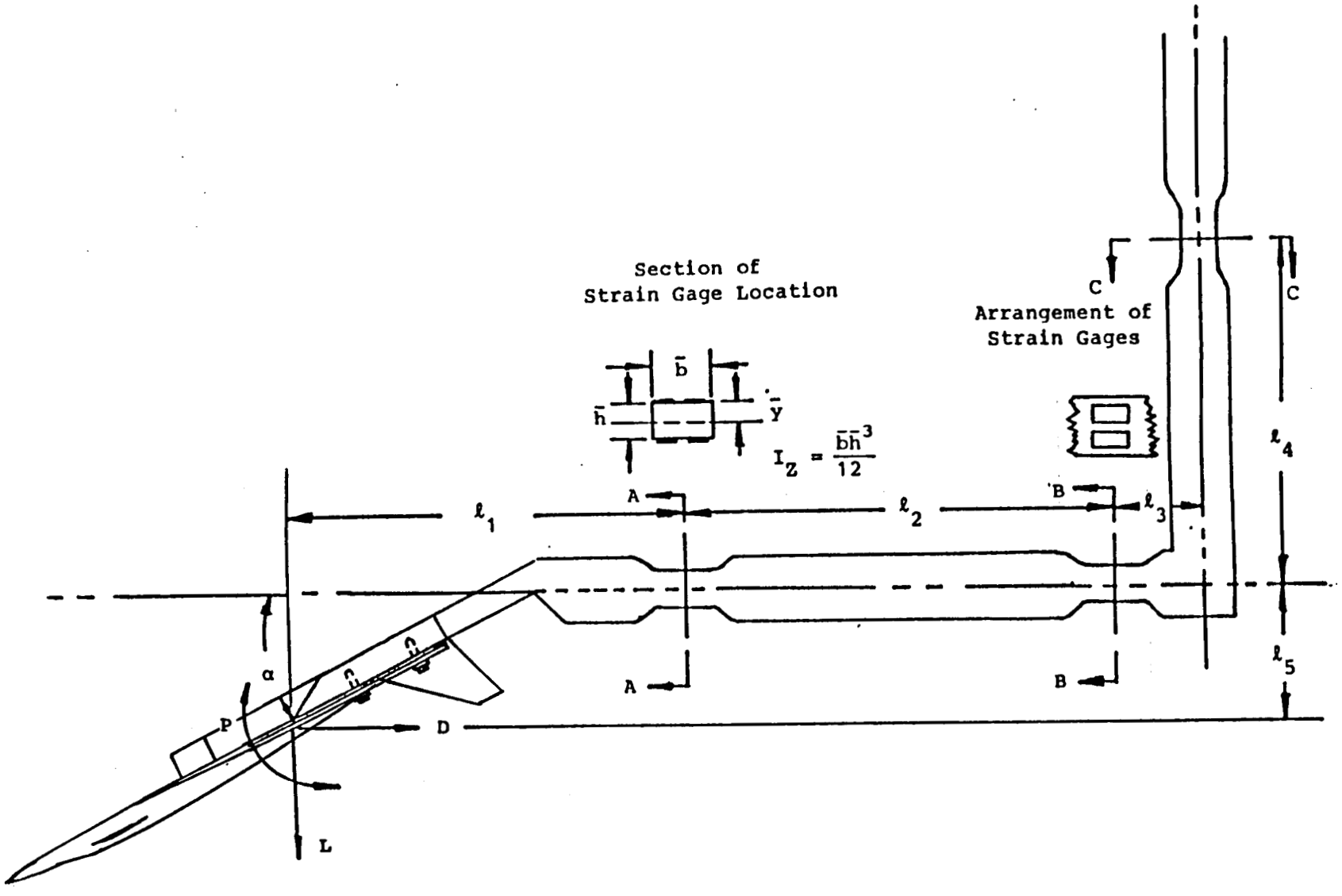

Figure 4: Sting Support and Strain Gage Arrangement

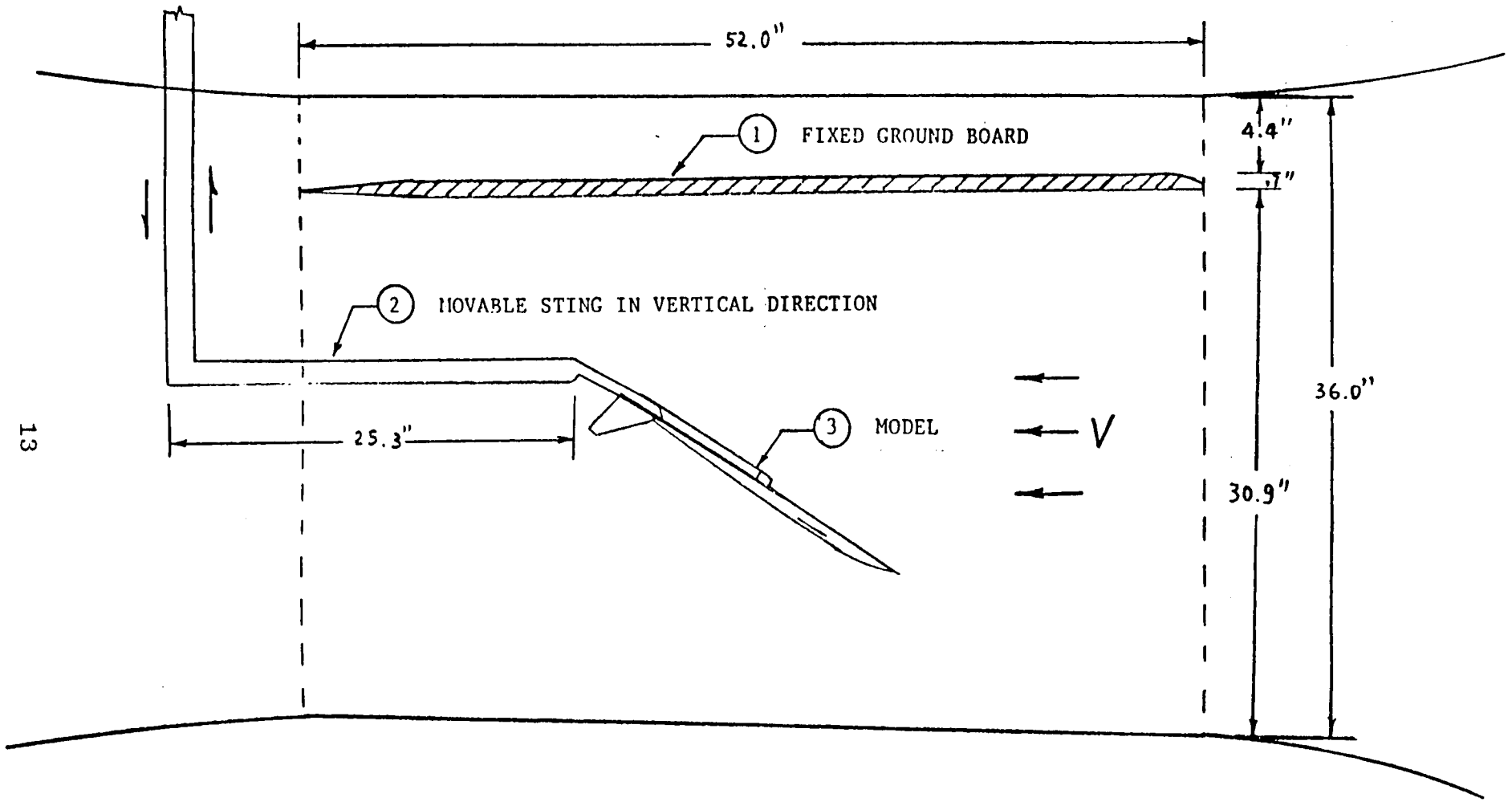

Figure 5: Test Section with Model Support and Ground Board in the KU Wind Tunnel

PHL

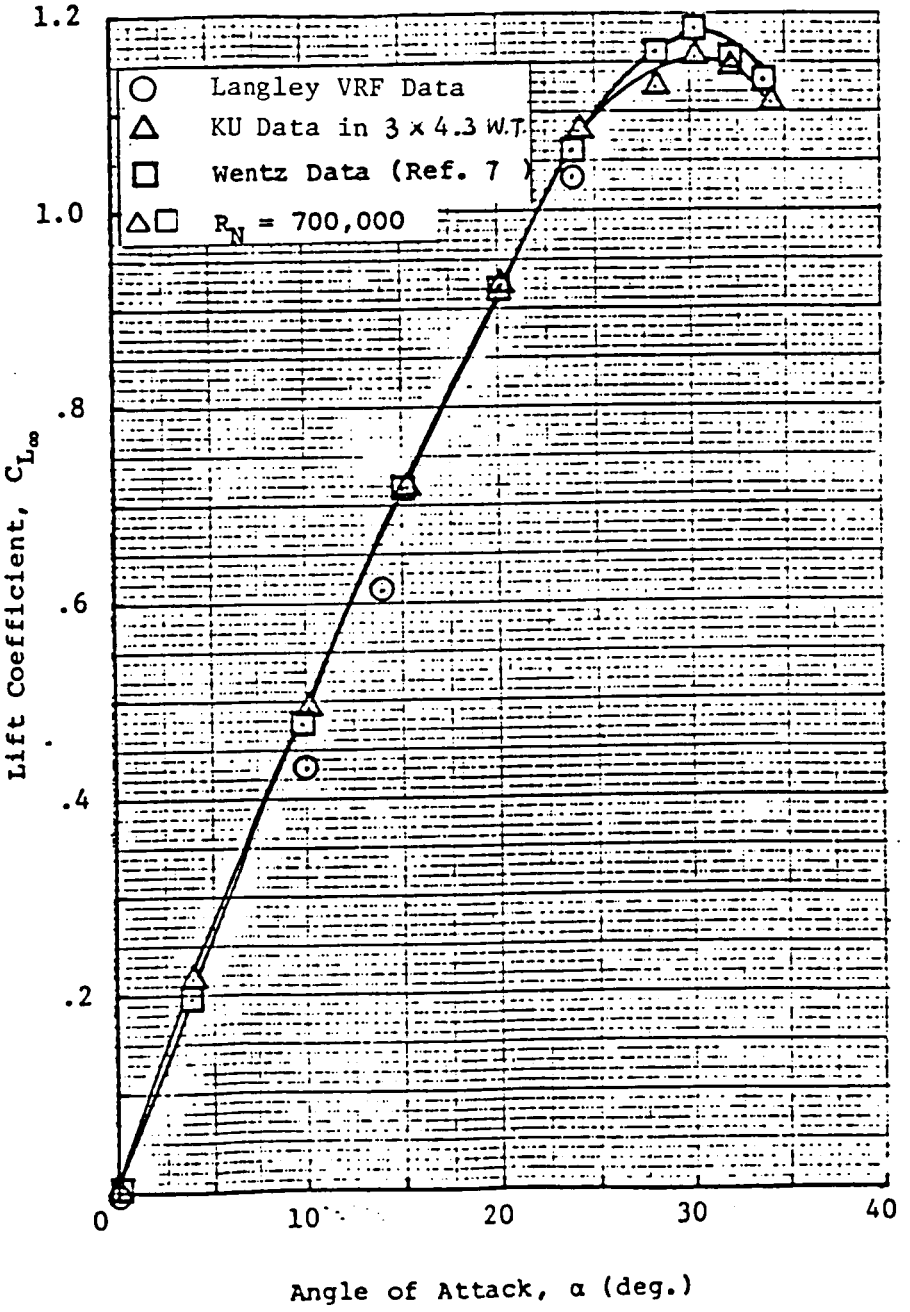

Figure 6A: Longitudinal Aerodynamic Characteristics for a 60-Degree Delta Wing in Out-of-Ground Effect

PHL.

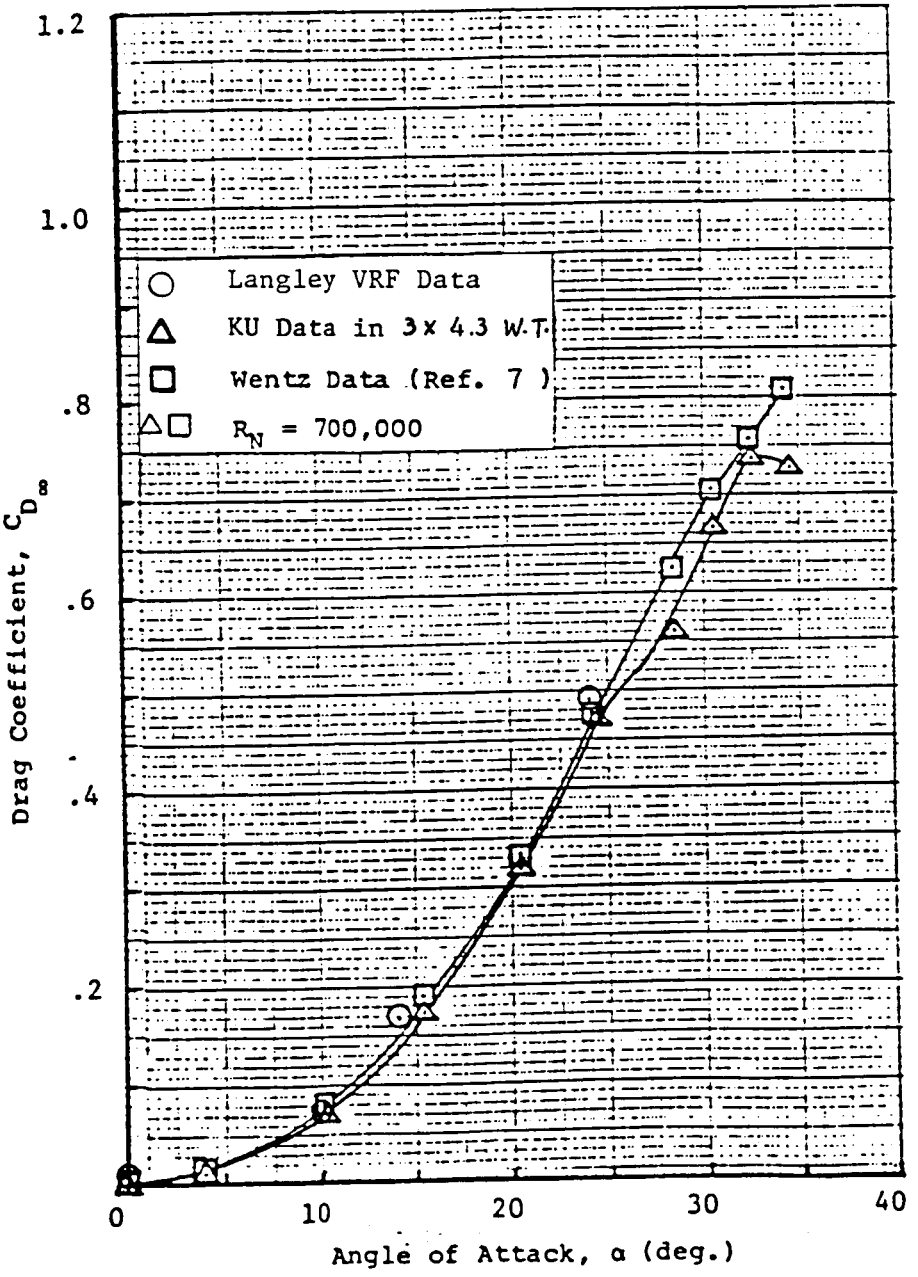

Figure 6B: Longitudinal Aerodynamic Characteristics for a 60-Degree Delta Wing in Out-of-Ground Effect

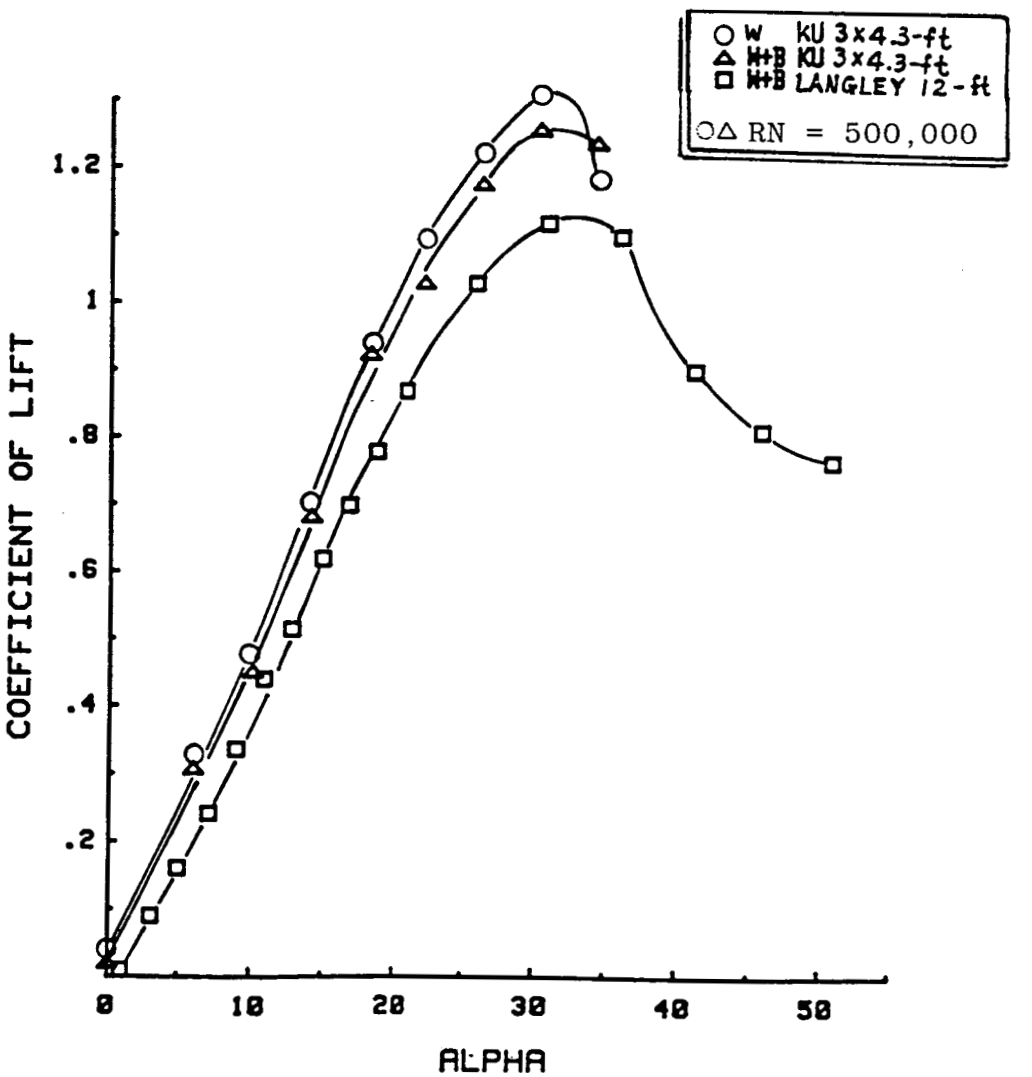

Figure 7A: Longitudinal Aerodynamic Characteristics for an F-106 Model in Out-of-Ground Effect

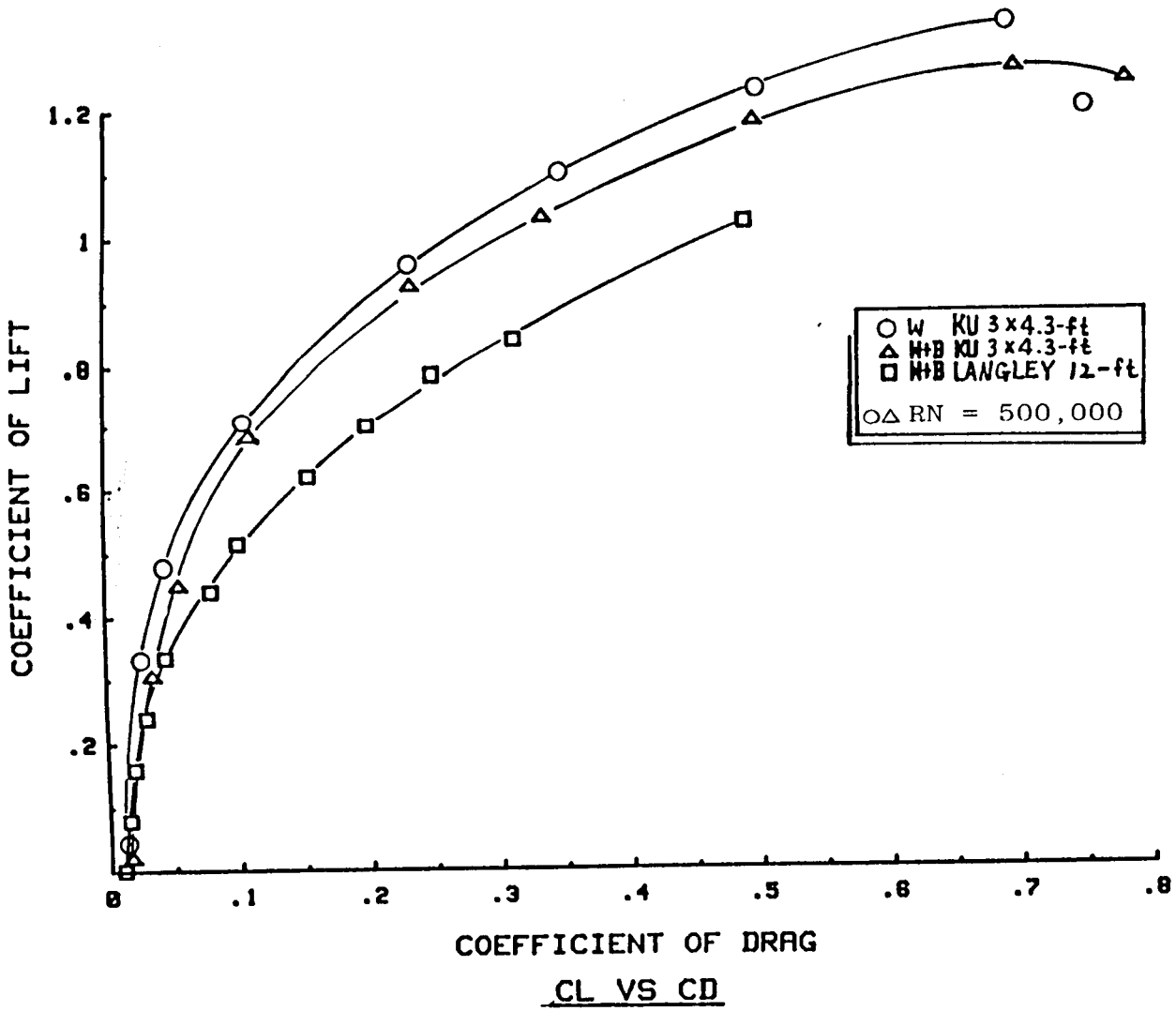

Figure 7B: Longitudinal Aerodynamic Characteristics for an F-106 Model in Out-of-Ground Effect

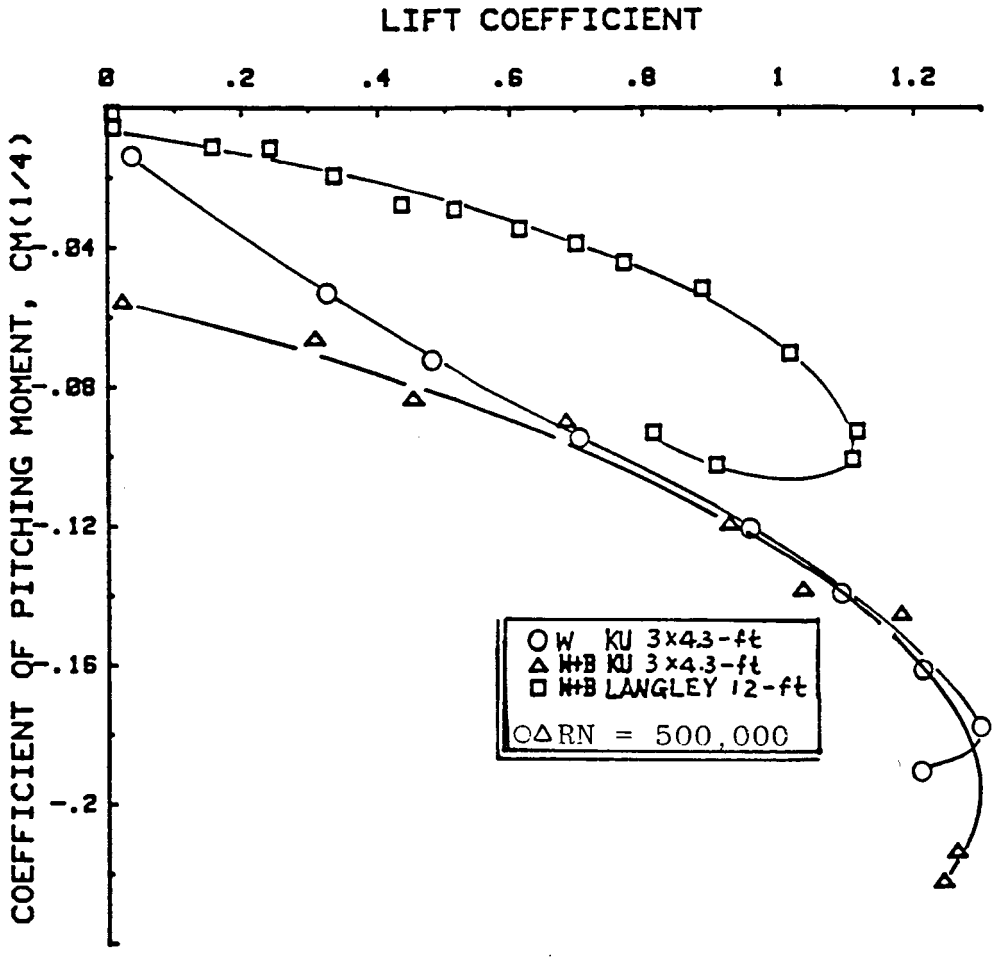

CM(1/4) VS CL

Figure 7C: Longitudinal Aerodynamic Characteristics for an F-106 Model in Out-of-Ground Effect

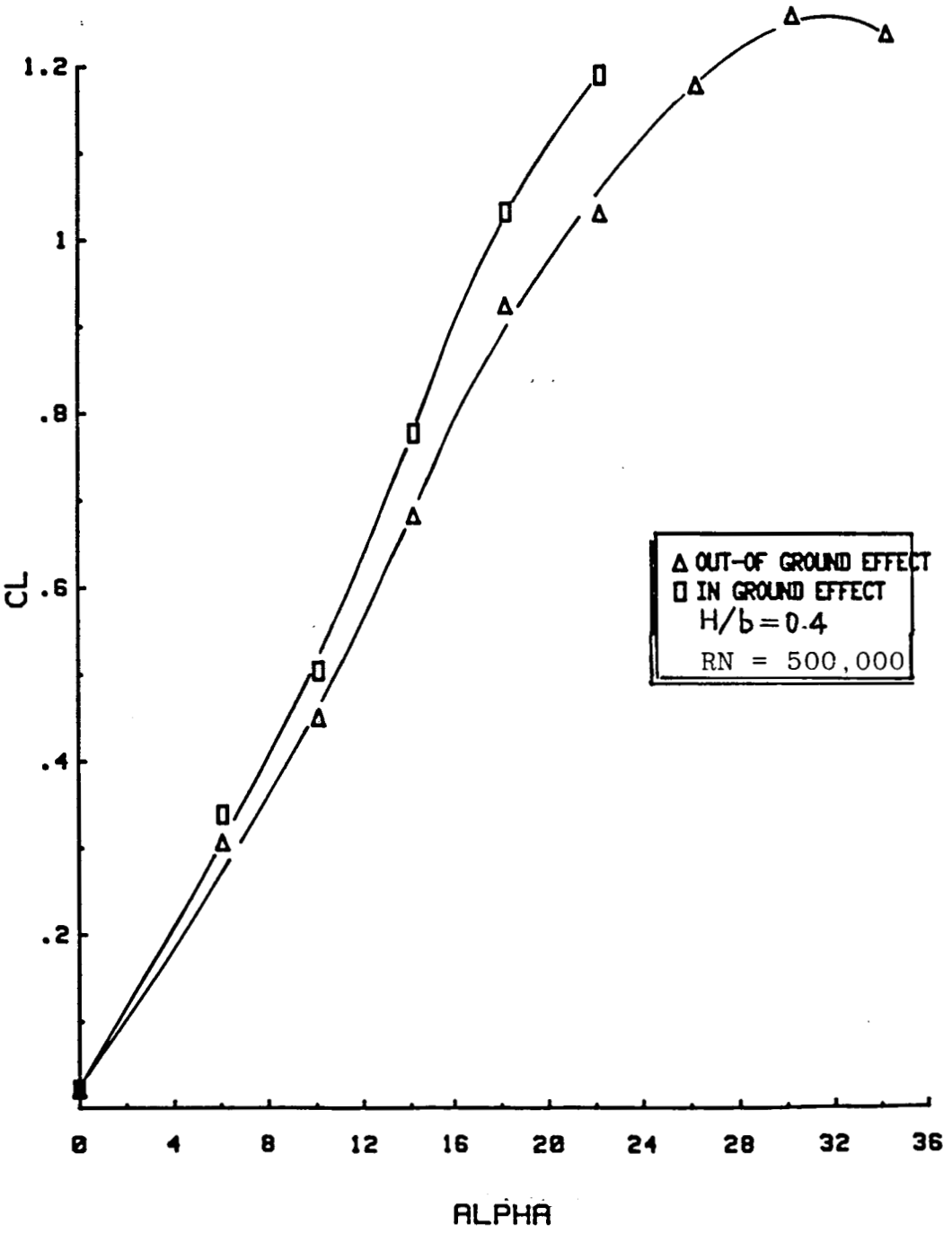

Figure 8A: Longitudinal Aerodynamic Characteristics for an F-106 Model in Static Ground Effect. H/b = 0.4.

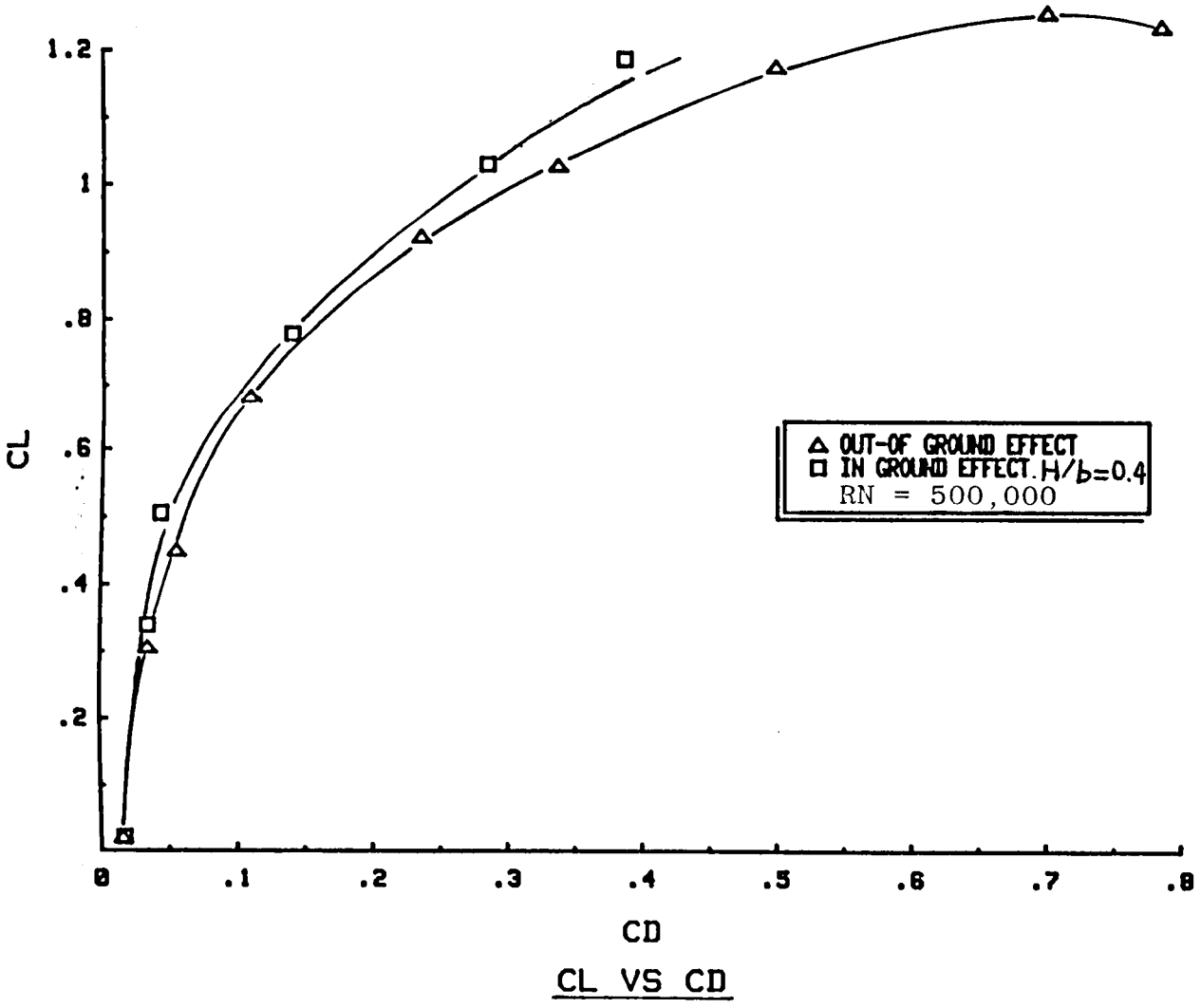

Figure 8B: Longitudinal Aerodynamic Characteristics for an F-106 Model in Static Ground Effect. H/b = 0.4.

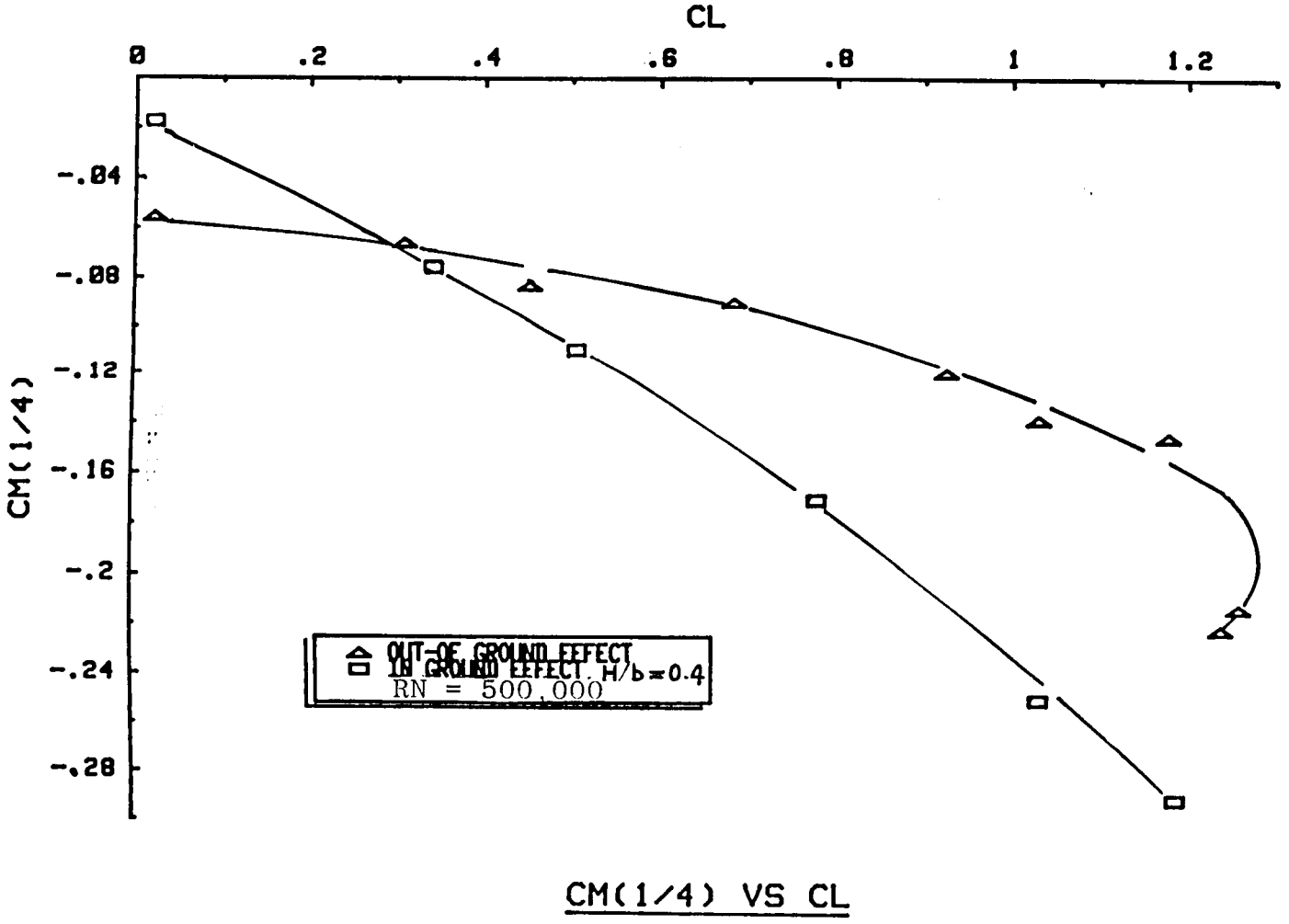

CM(1/4) VS CL

Figure 8C: Longitudinal Aerodynamic Characteristics for an F-106 Model in Static Ground Effect. H/b = 0.4.

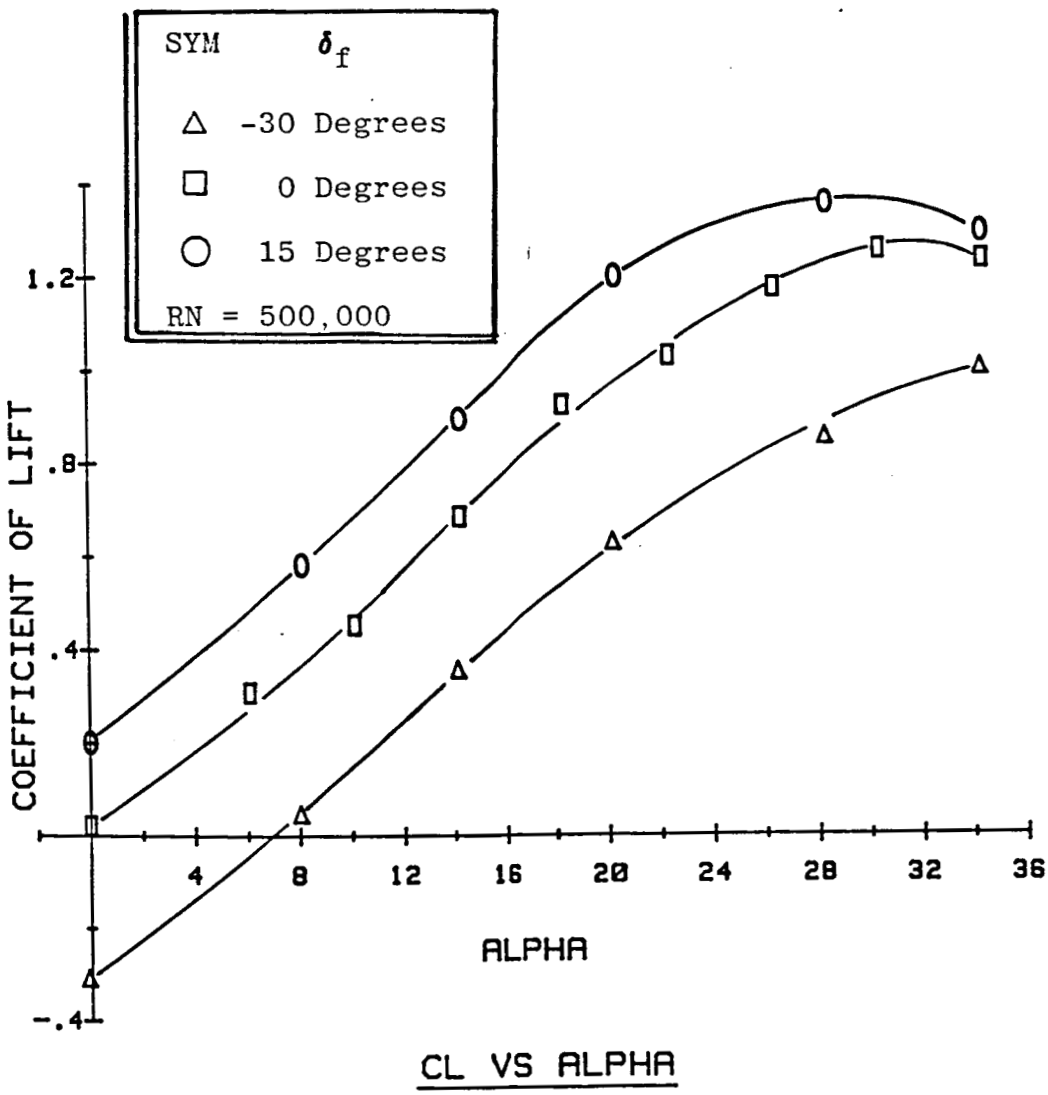

Figure 9A: Longitudinal Aerodynamic Characteristics for an F-106 Model in Out-of-Ground Effect with Flap Deflections

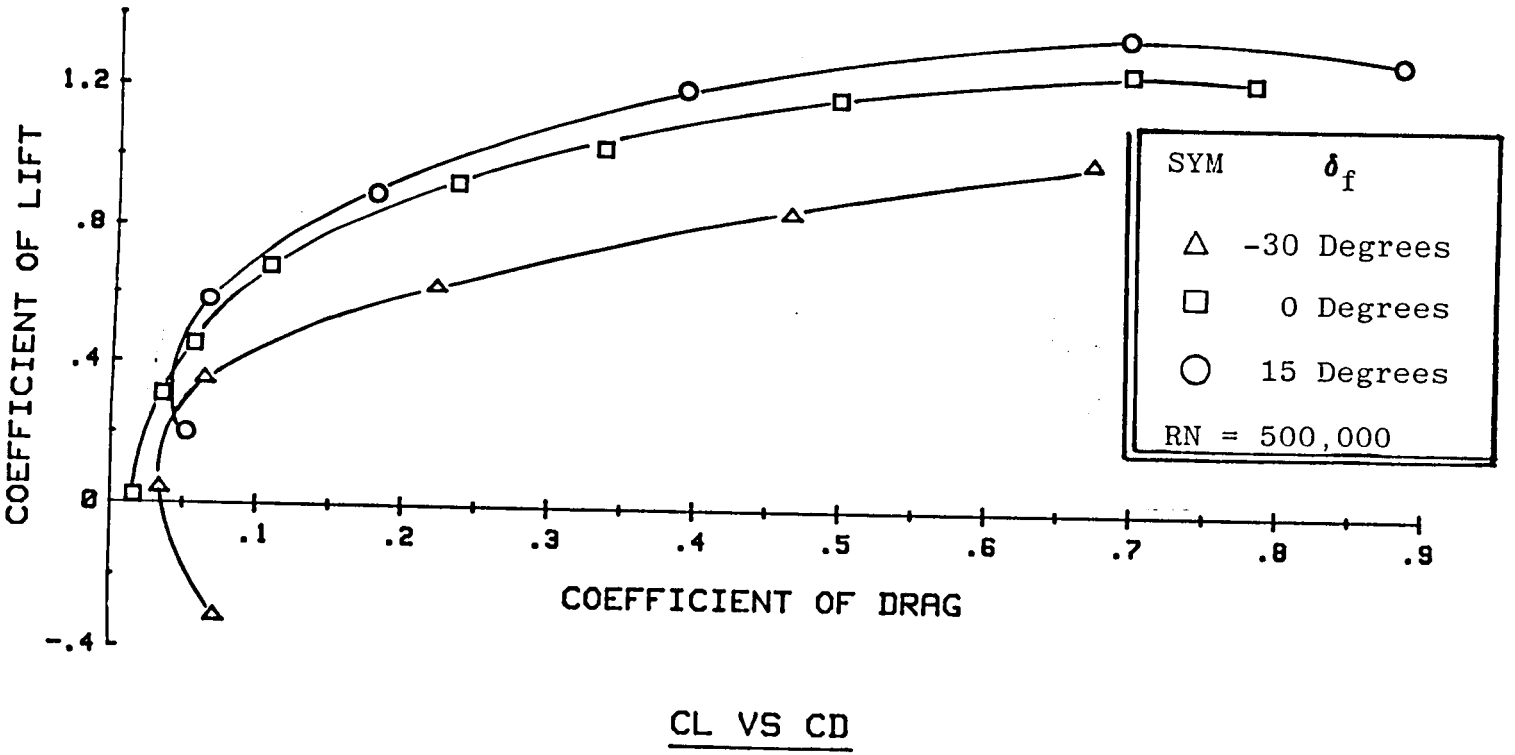

CL VS CD

Figure 9B: Longitudinal Aerodynamic Characteristics for an F-106 Model in Out-of-Ground Effect with Flap Deflections

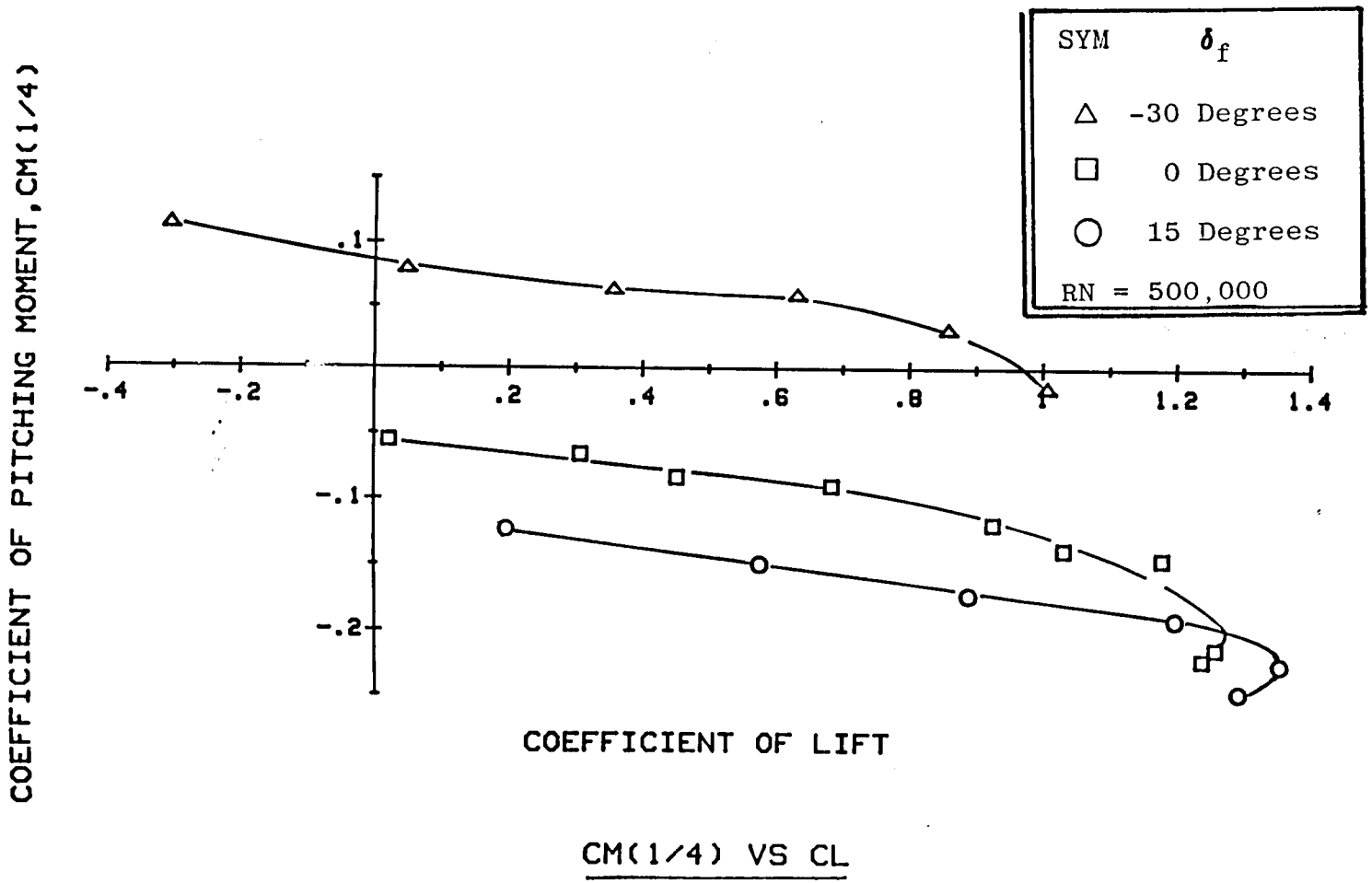

Figure 9C: Longitudinal Aerodynamic Characteristics for an F-106 Model in Out-of-Ground Effect with Flap Deflections

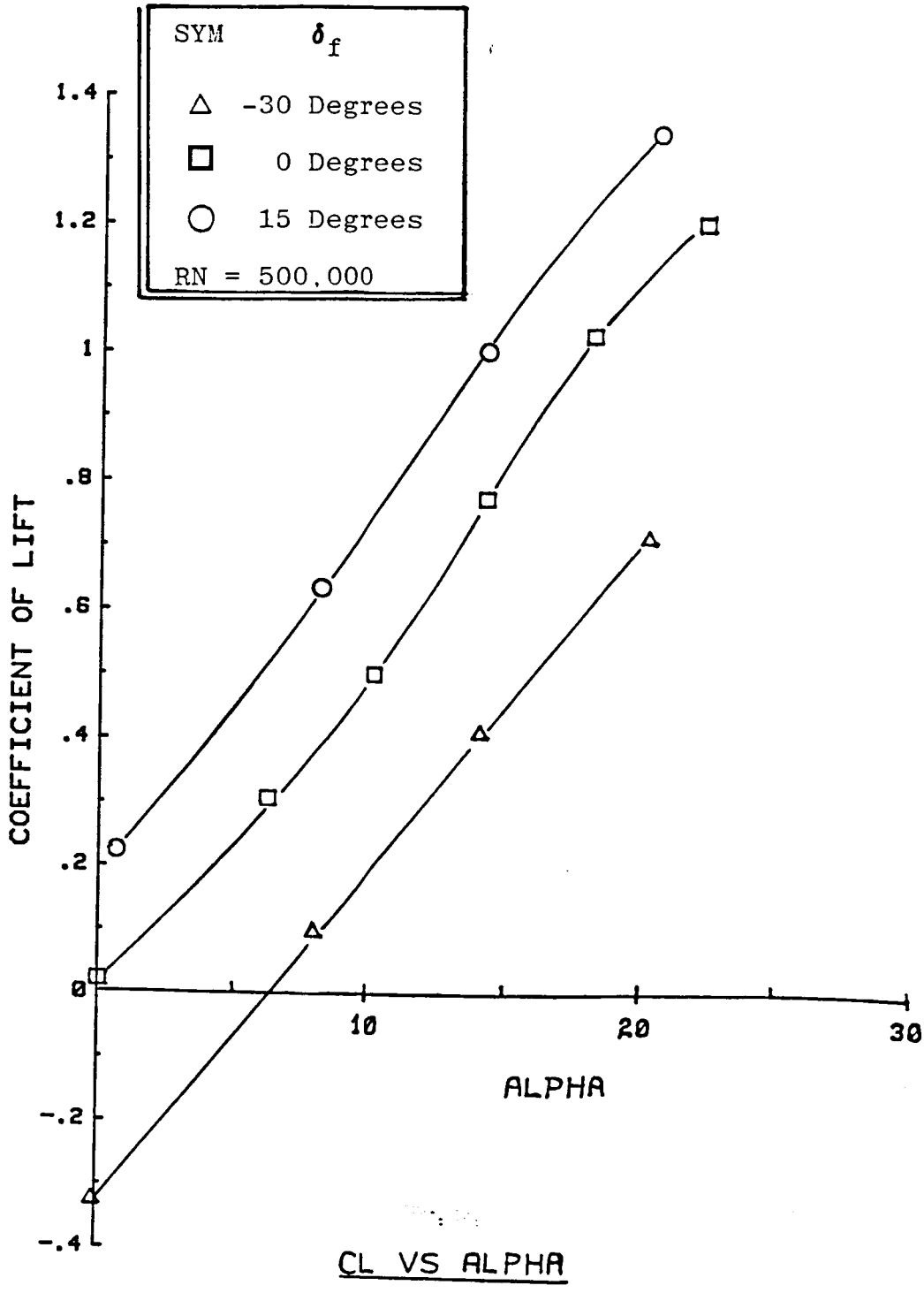

Figure 10A: Longitudinal Aerodynamic Characteristics for an F-106 Model with Flap Deflections in Static Ground Effect. H/b = 0.4.

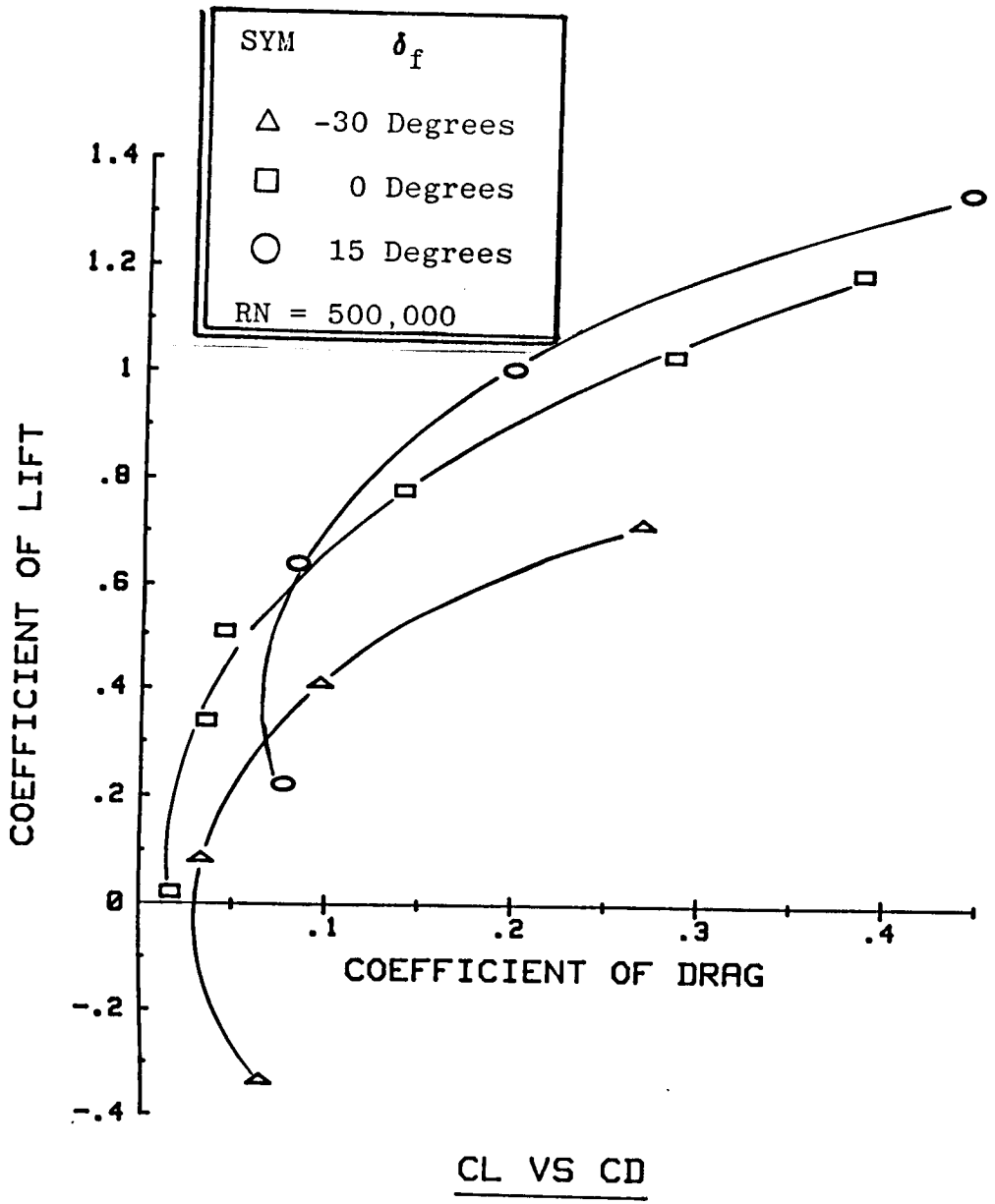

Figure 10B: Longitudinal Aerodynamic Characteristics for an F-106 Model with Flap Deflections in Static Ground Effect. H/b = 0.4.

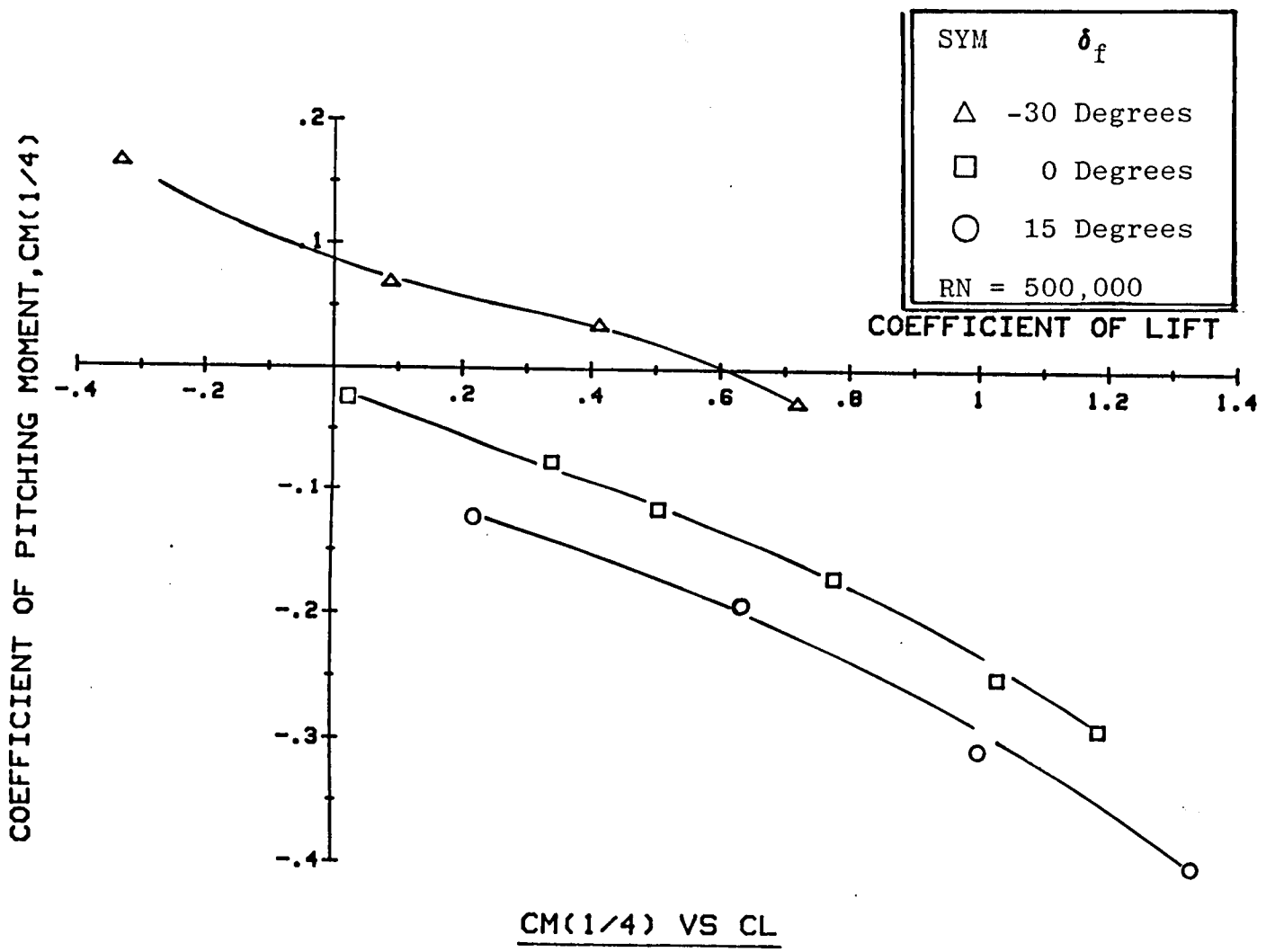

Figure 10C: Longitudinal Aerodynamic Characteristics for an F-106 Model with Flap Deflections in Static Ground Effect. H/b = 0.4.

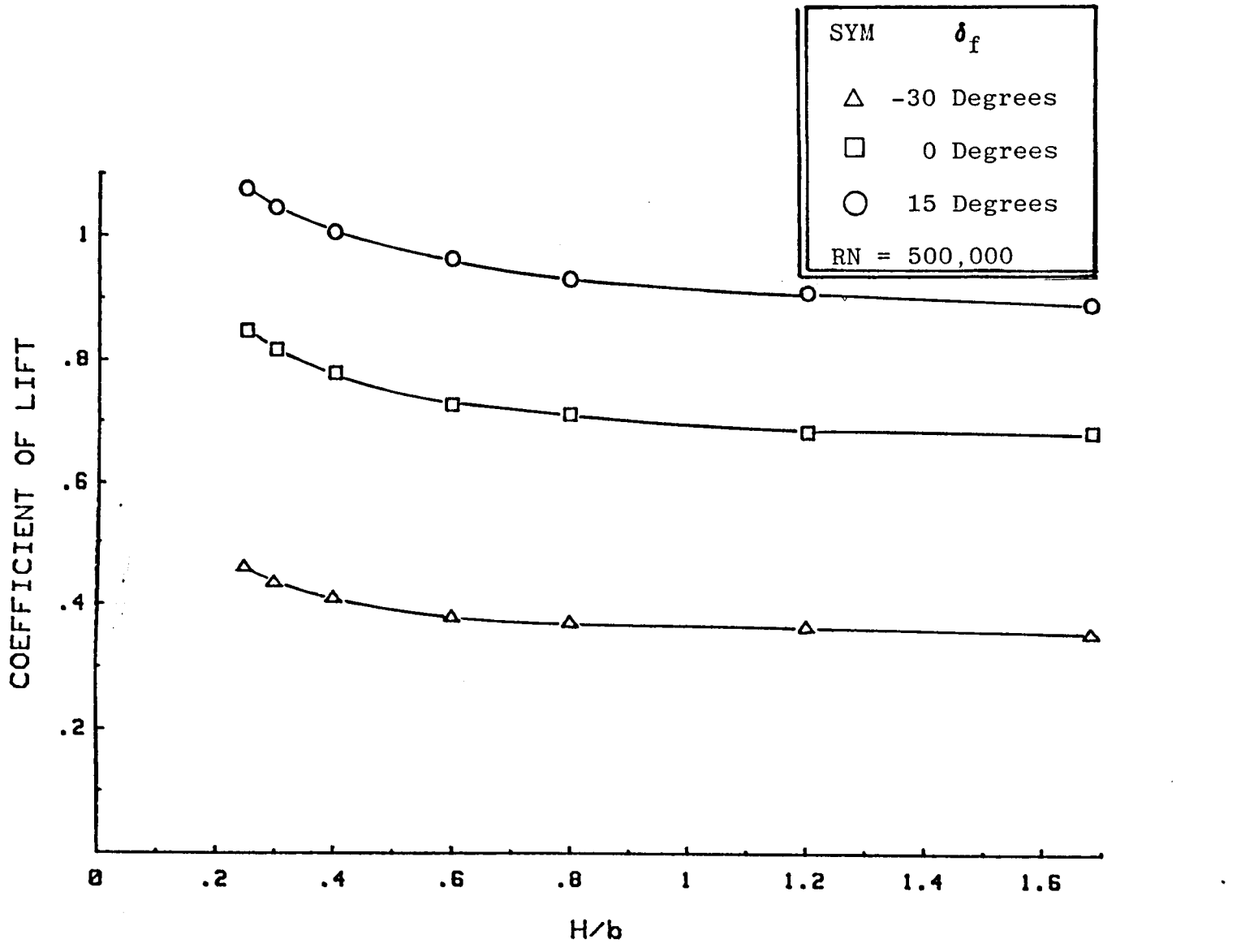

Figure 11A: Longitudinal Aerodynamic Characteristics for an F-106 Model with Flap Deflections in Static Ground Effect at Different Ground Heights. α = 14 Degrees.

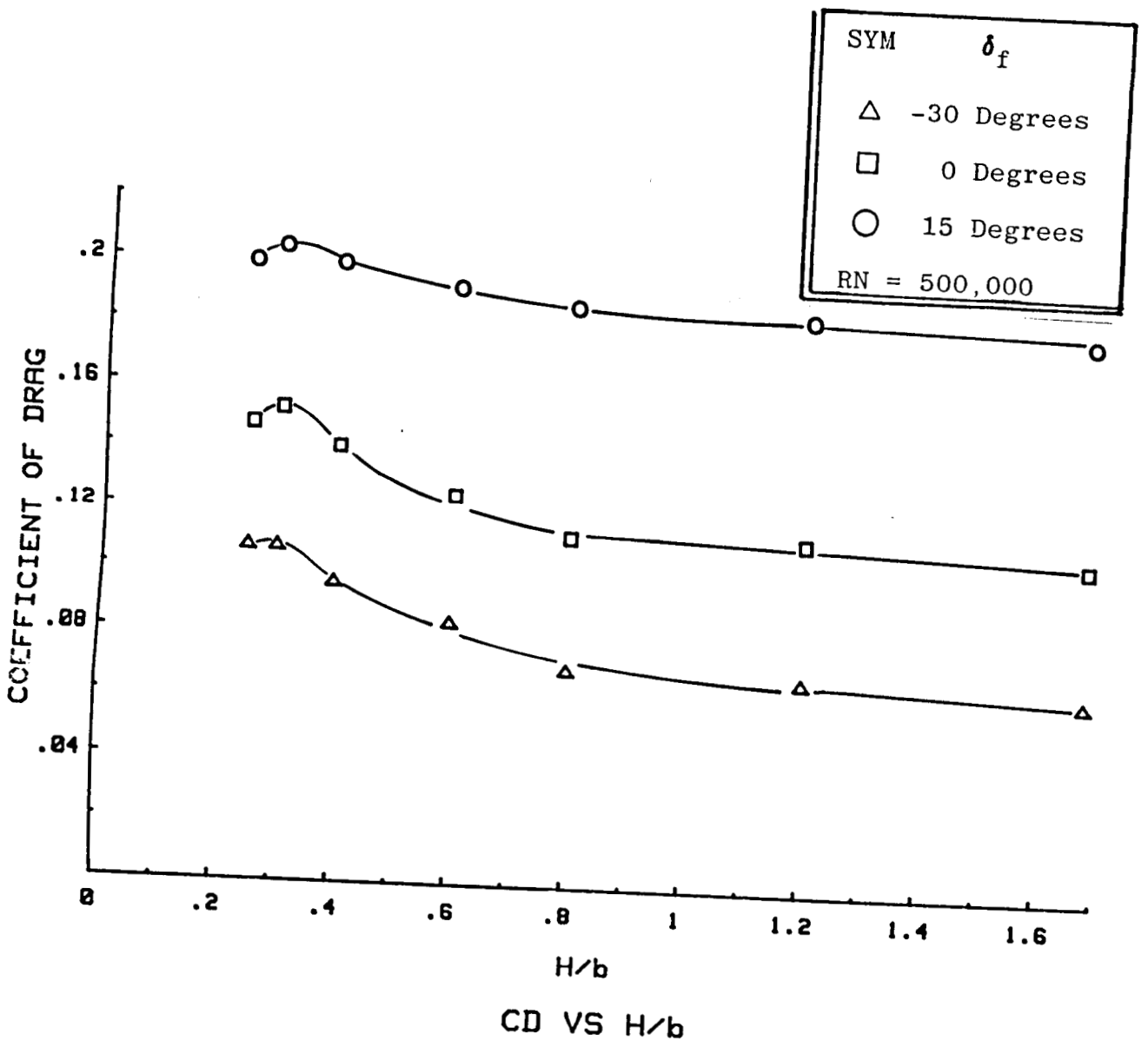

Figure 11B: Longitudinal Aerodynamic Characteristics for an F-106 Model with Flap Deflections in Static Ground Effect at Different Ground Heights. α = 14 Degrees.

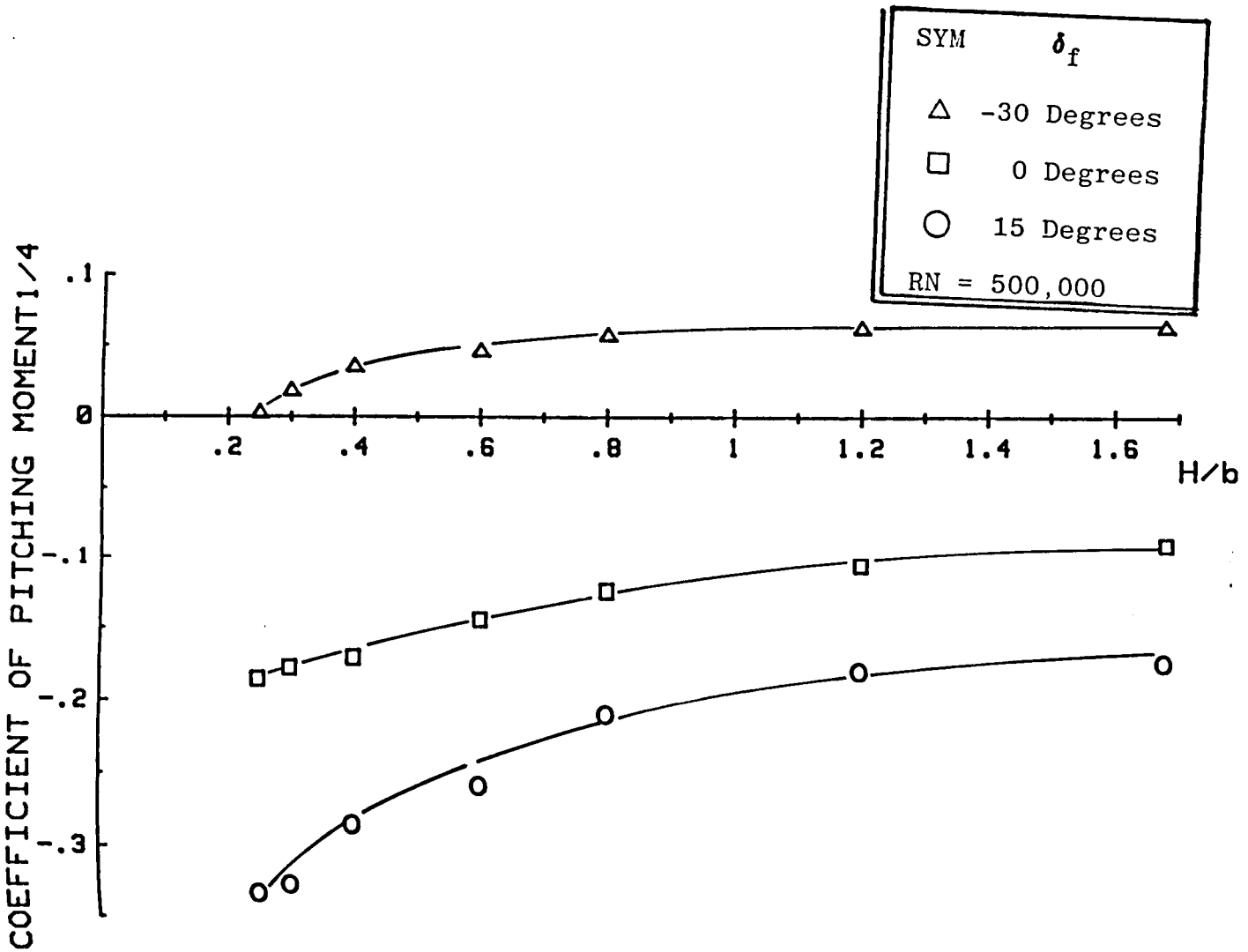

CM1/4 VS H/b

Figure 11C: Longitudinal Aerodynamic Characteristics for an F-106 Model with Flap Deflections in Static Ground Effect at Different Ground Heights. α = 14 Degrees.

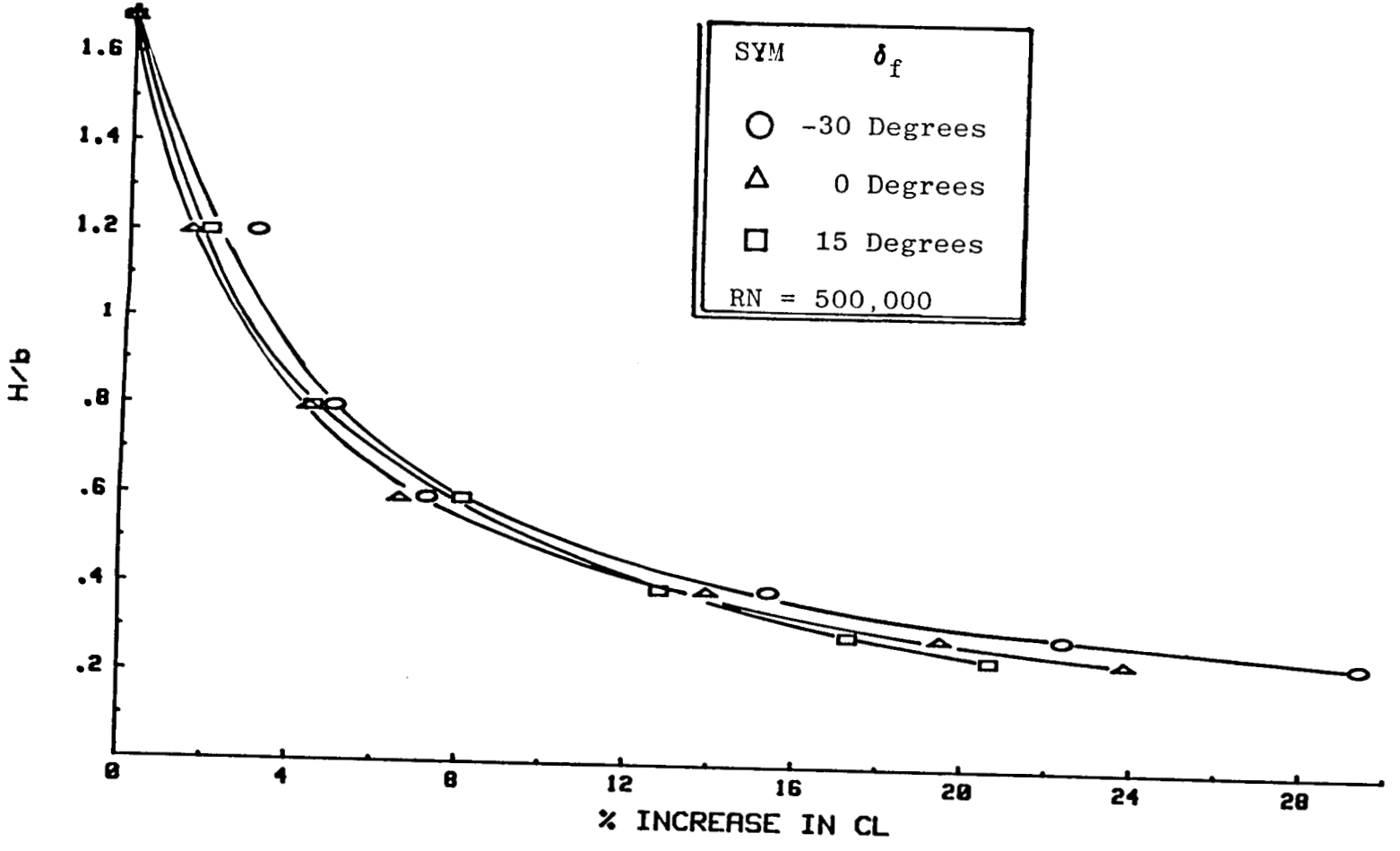

H/b VS ΔCL%

Figure 12A: Incremental Lift and Drag for an F-106 Model with Flap Deflections in Static Ground Effect at α = 14 Degrees.

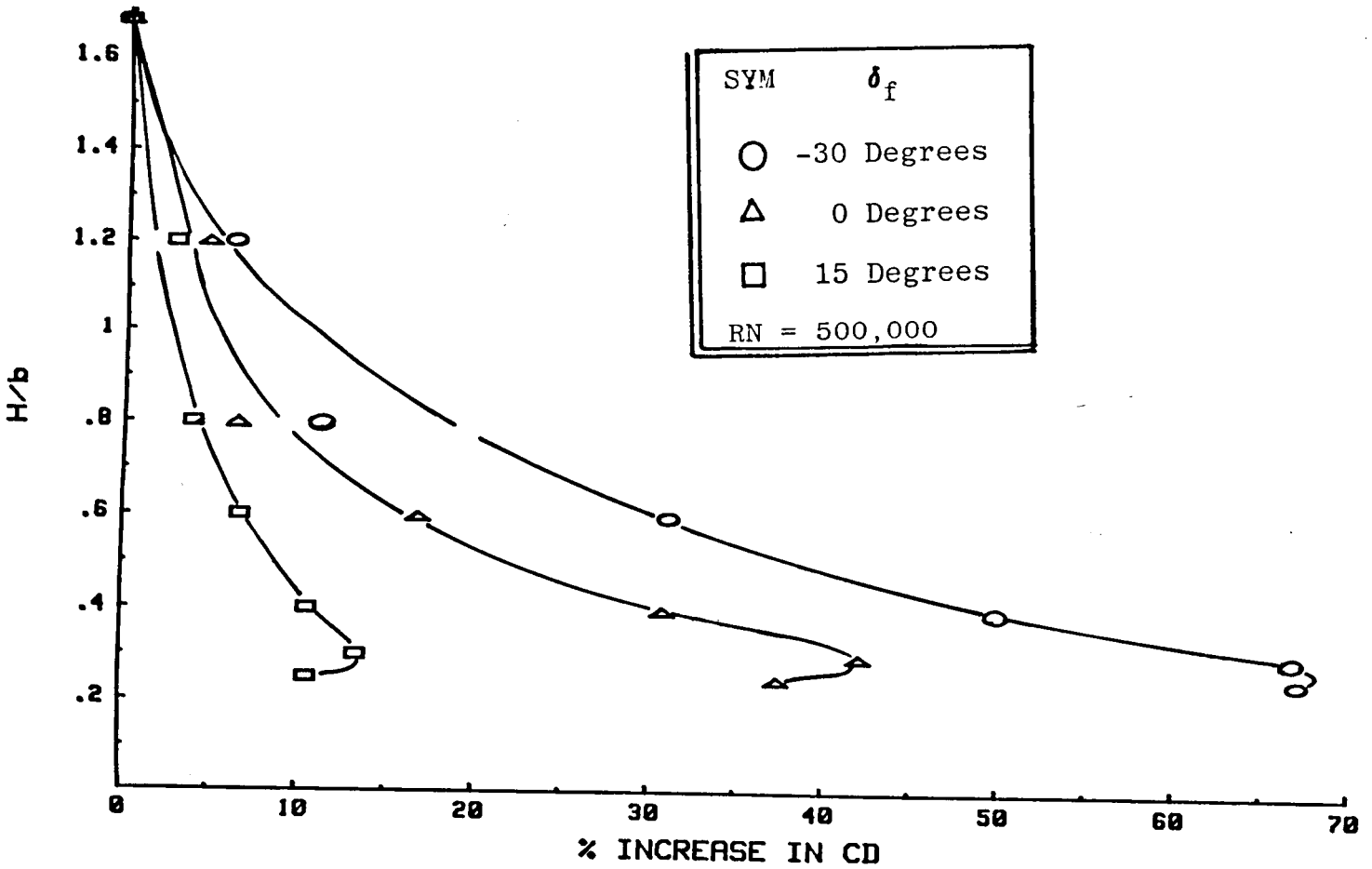

H/b VS ΔCD%

Figure 12B: Incremental Lift and Drag for an F-106 Model with Flap Deflections in Static Ground Effect at α = 14 Degrees.

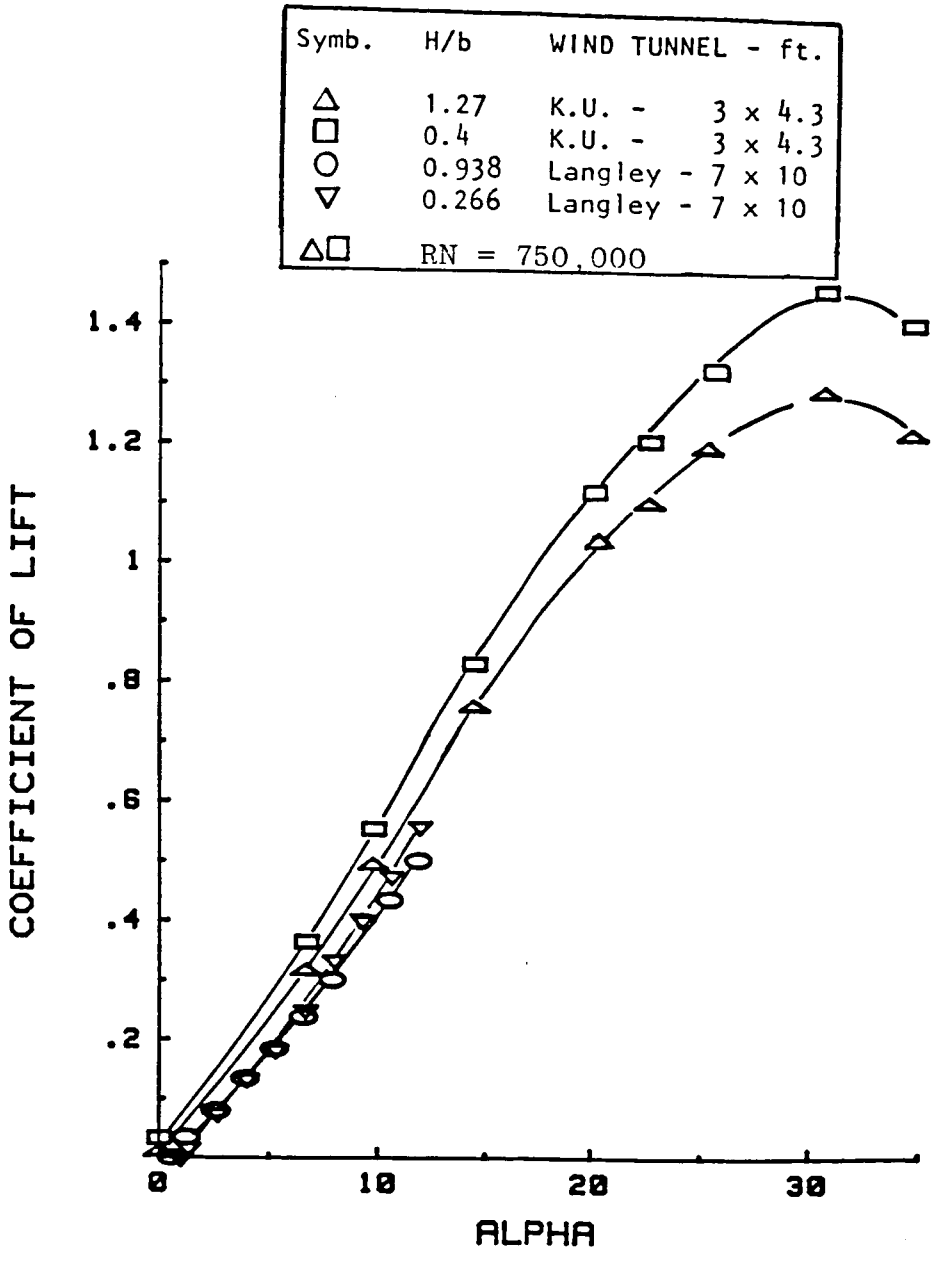

Figure 13A: Comparison of Some Static Ground Effect Data for the XB-70-1 Configuration from the KU and Langley 7 x 10 Tunnels

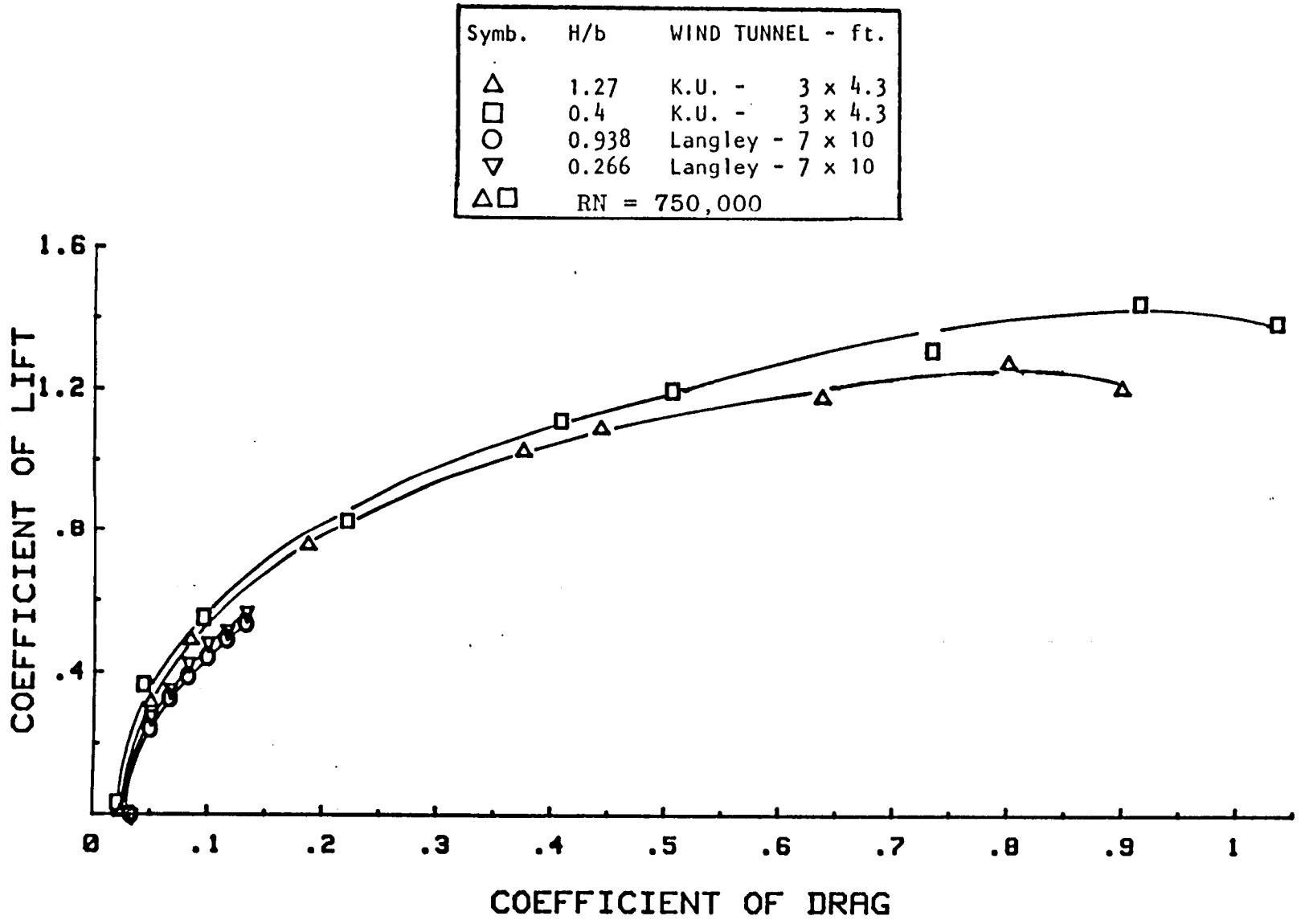

Figure 13B: Comparison of Some Static Ground Effect Data for the XB-70-1 Configuration from the KU and Langley 7 x 10 Tunnels

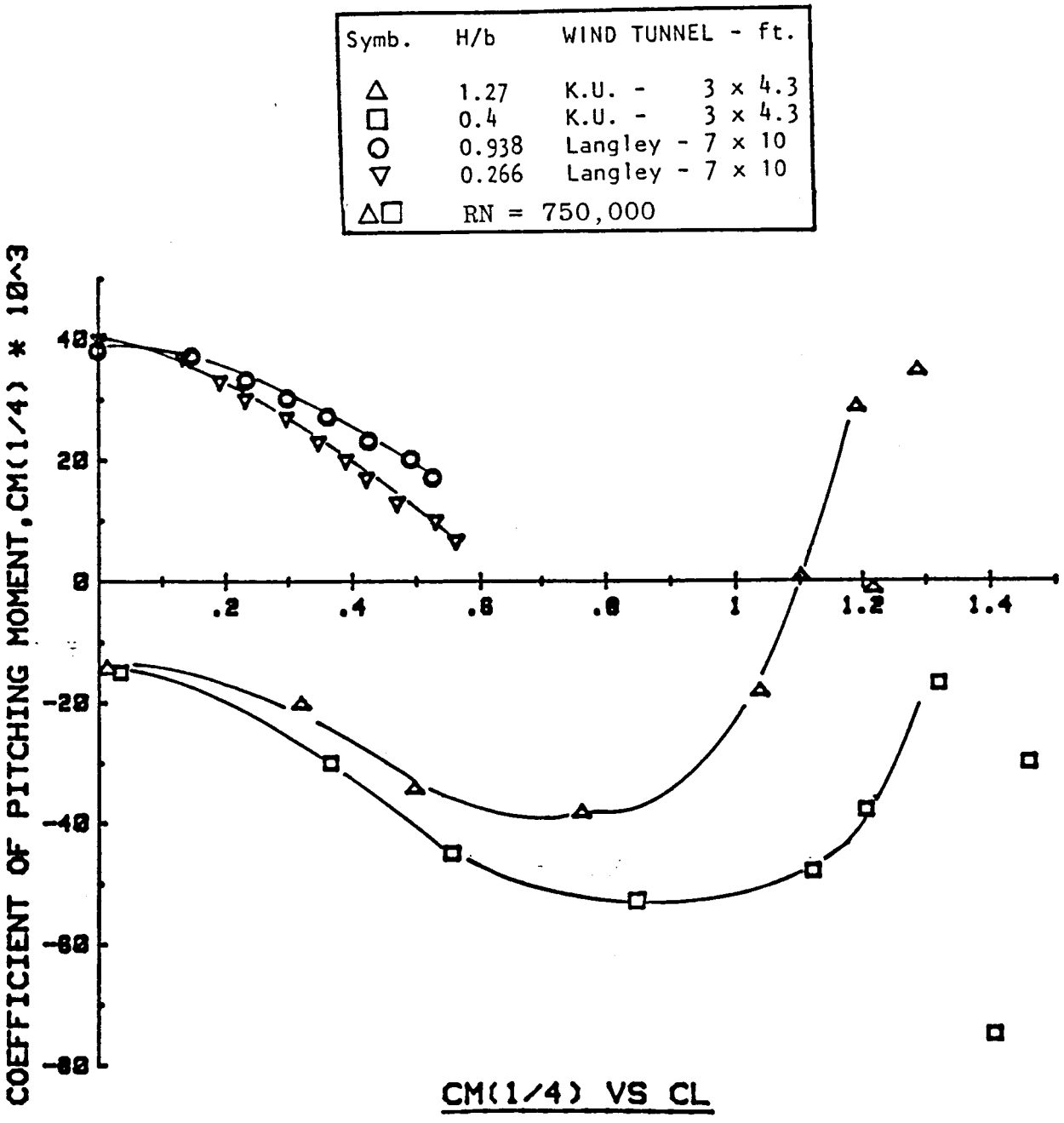

Figure 13C: Comparison of Some Static Ground Effect Data for the XB-70-1 Configuration from the KU and Langley 7 x 10 Tunnels

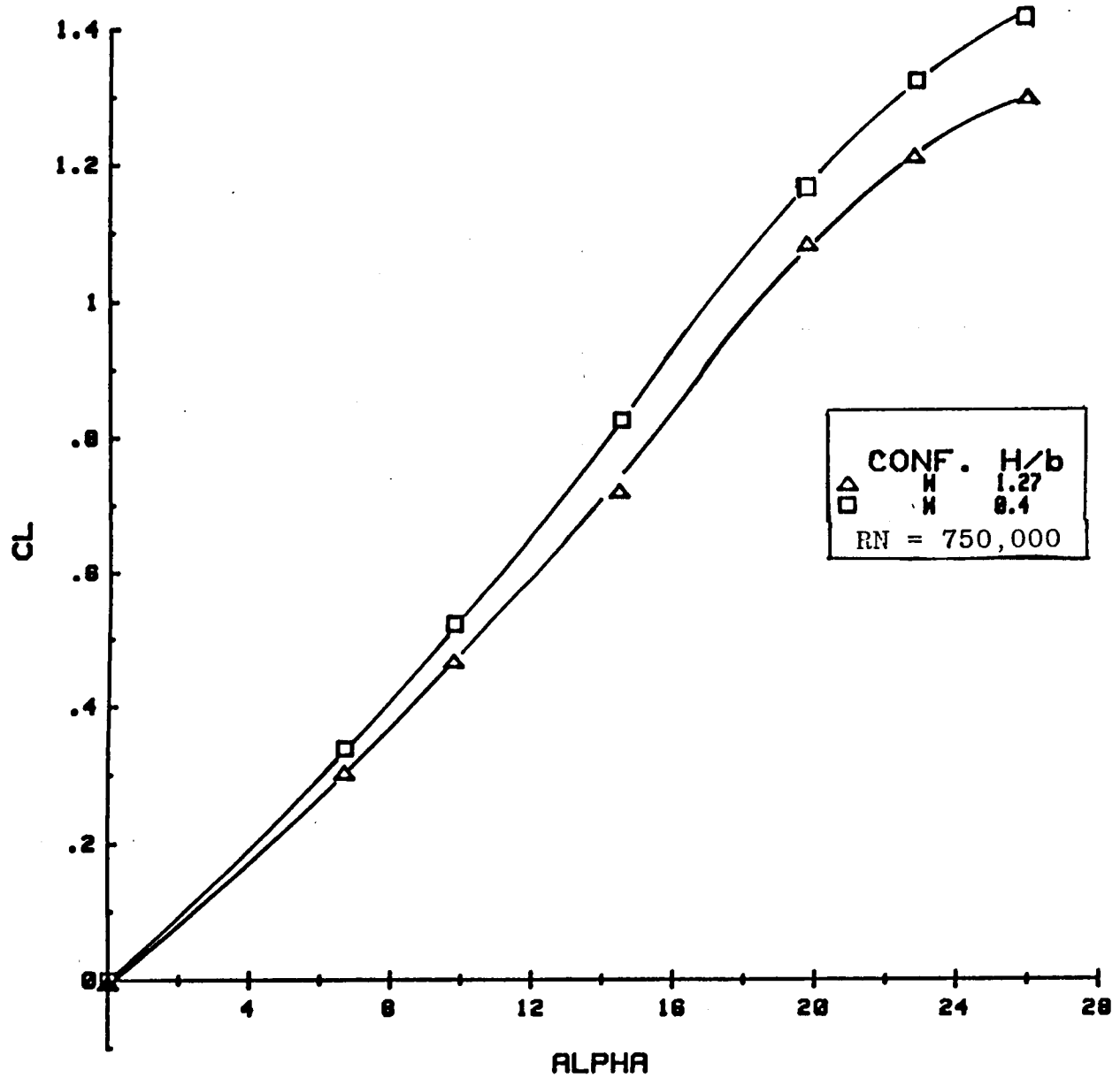

Figure 14A: Longitudinal Aerodynamic Characteristics for an XB-70-1 Model with Wing Alone in Static Ground Effect

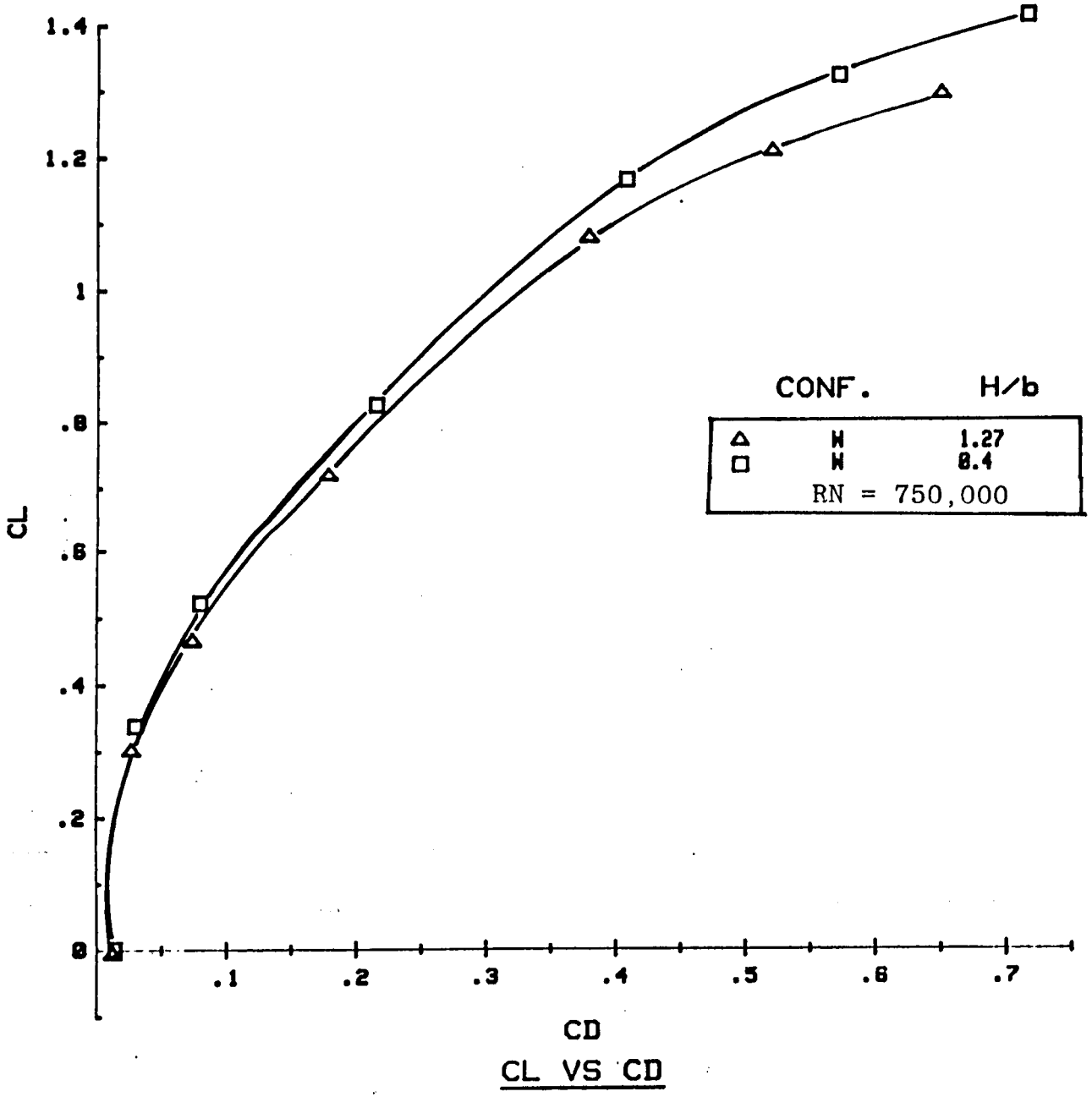

Figure 14B: Longitudinal Aerodynamic Characteristics for an XB-70-1 Model with Wing Alone in Static Ground Effect

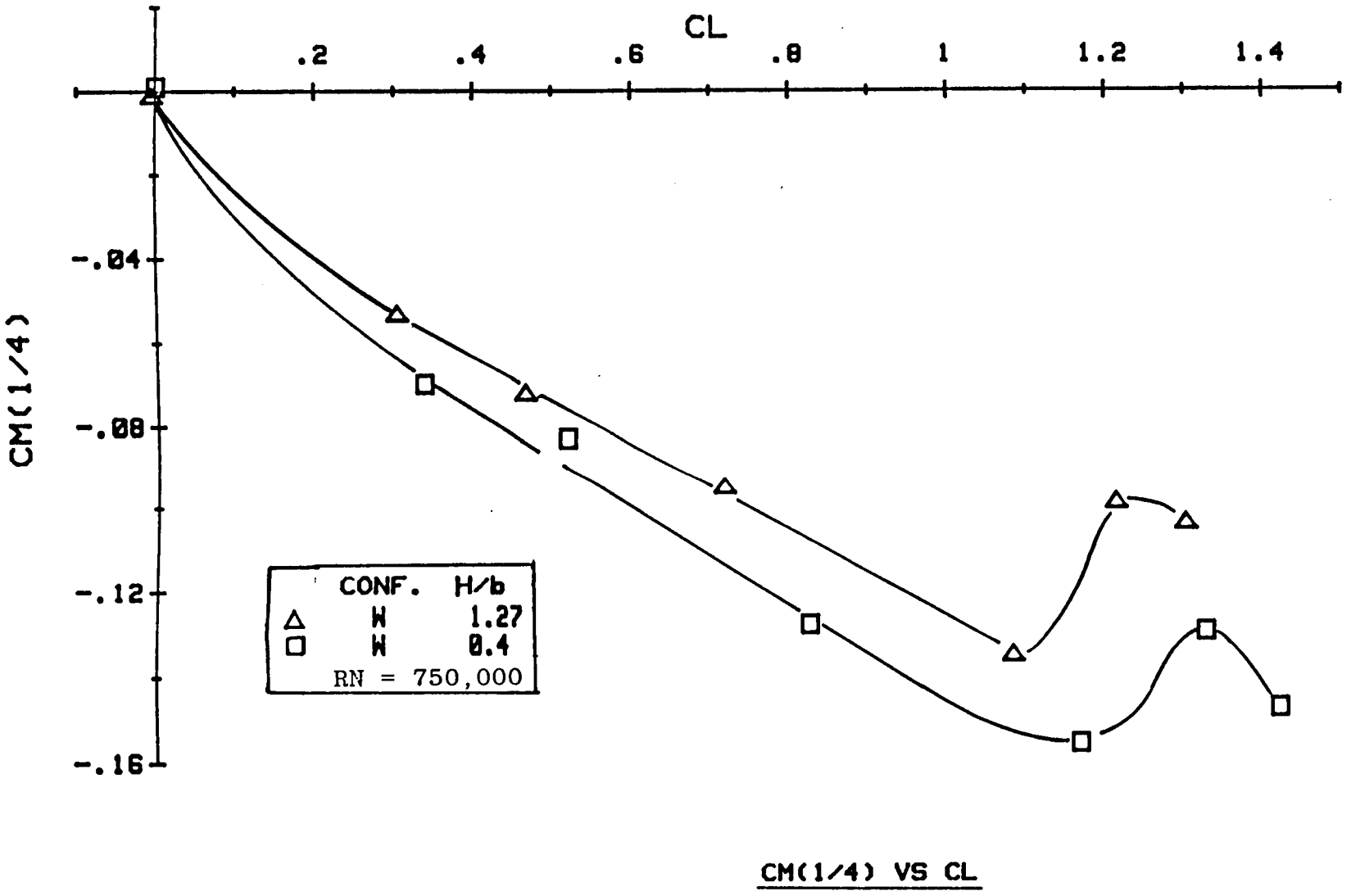

Figure 14C: Longitudinal Aerodynamic Characteristics for an XB-70-1 Model with Wing Alone in Static Ground Effect

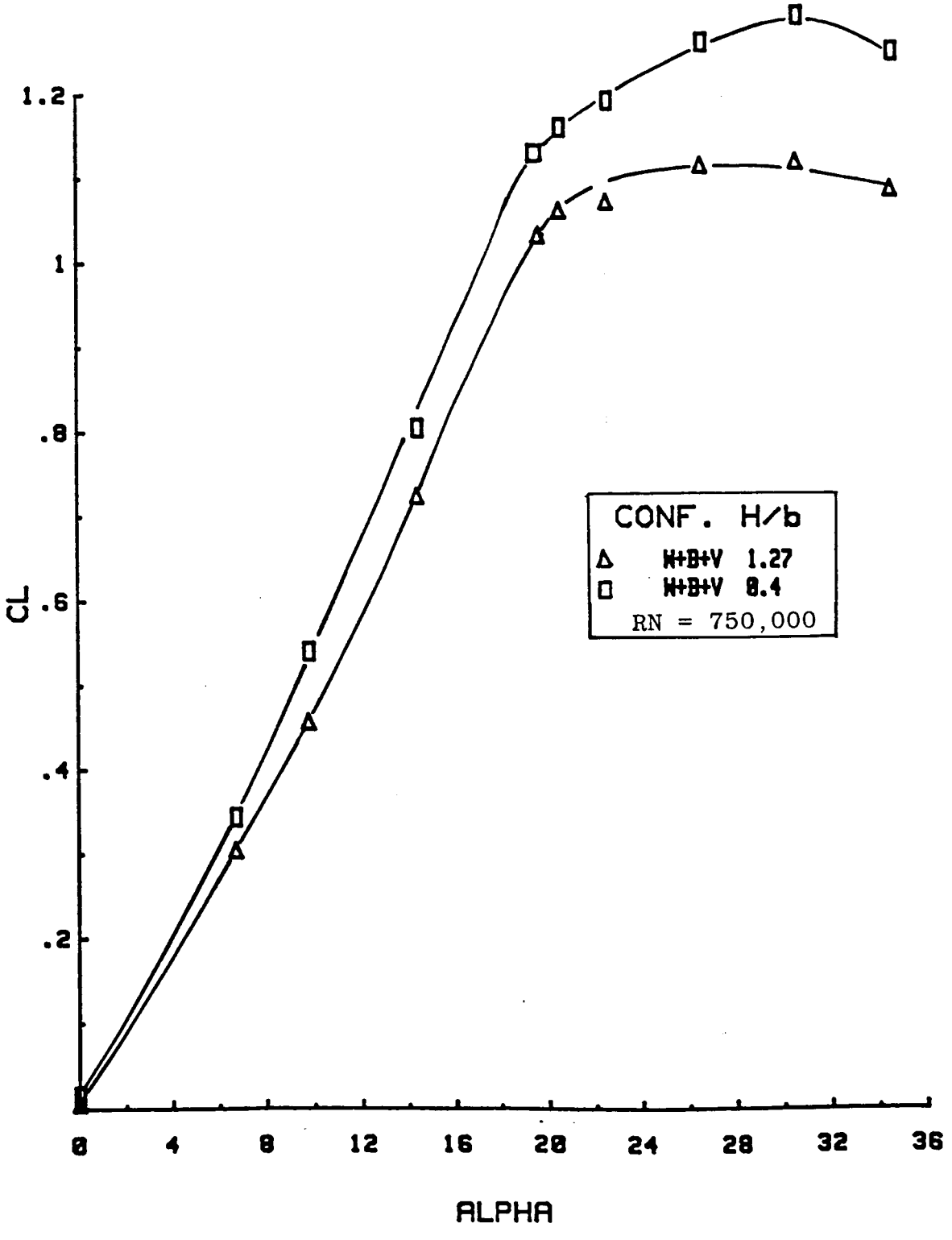

Figure 15A: Longitudinal Aerodynamic Characteristics for an XB-70-1 Model (W + B + V) in Static Ground Effect

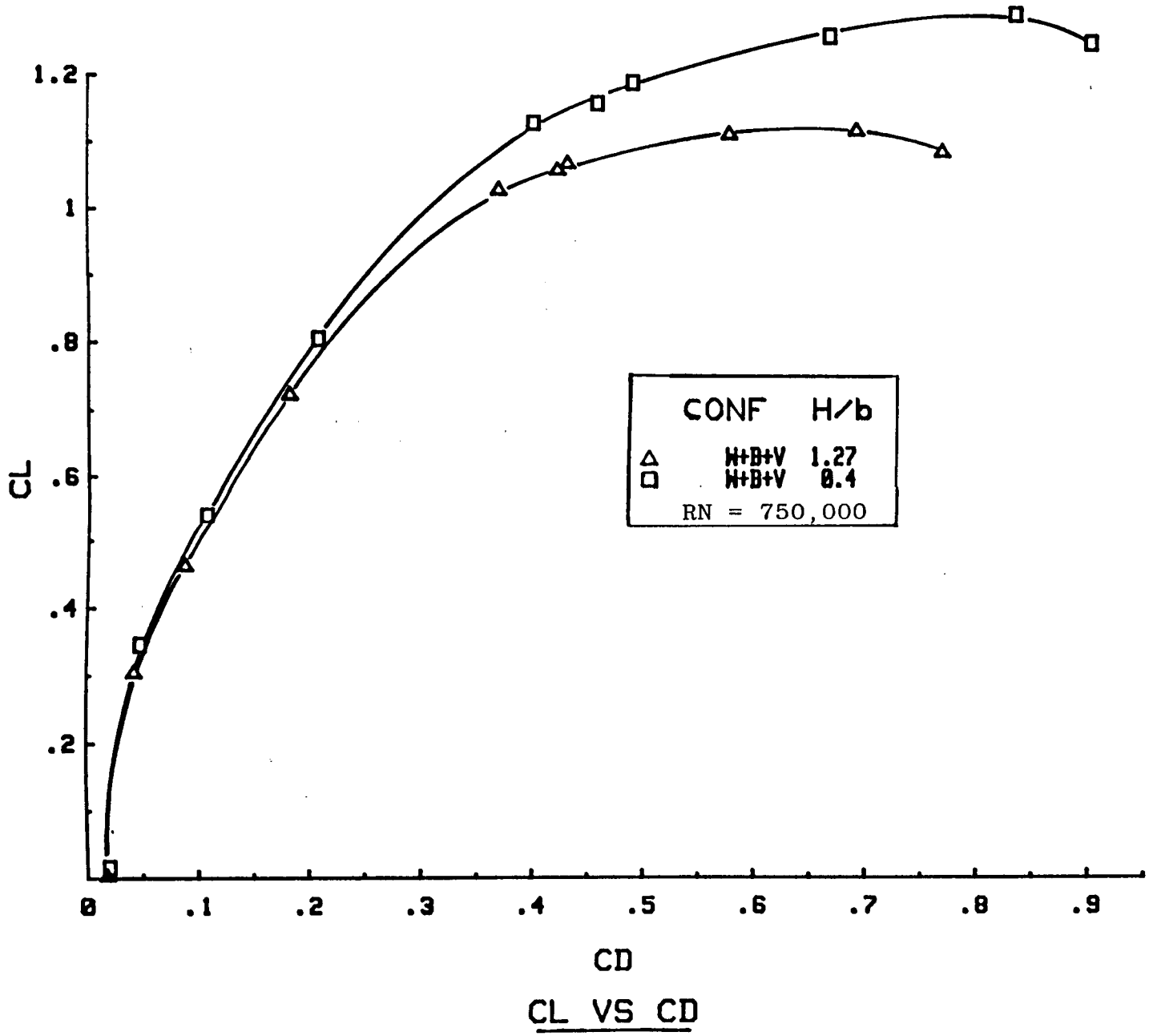

Figure 15B: Longitudinal Aerodynamic Characteristics for an XB-70-1 Model (W + B + V) in Static Ground Effect

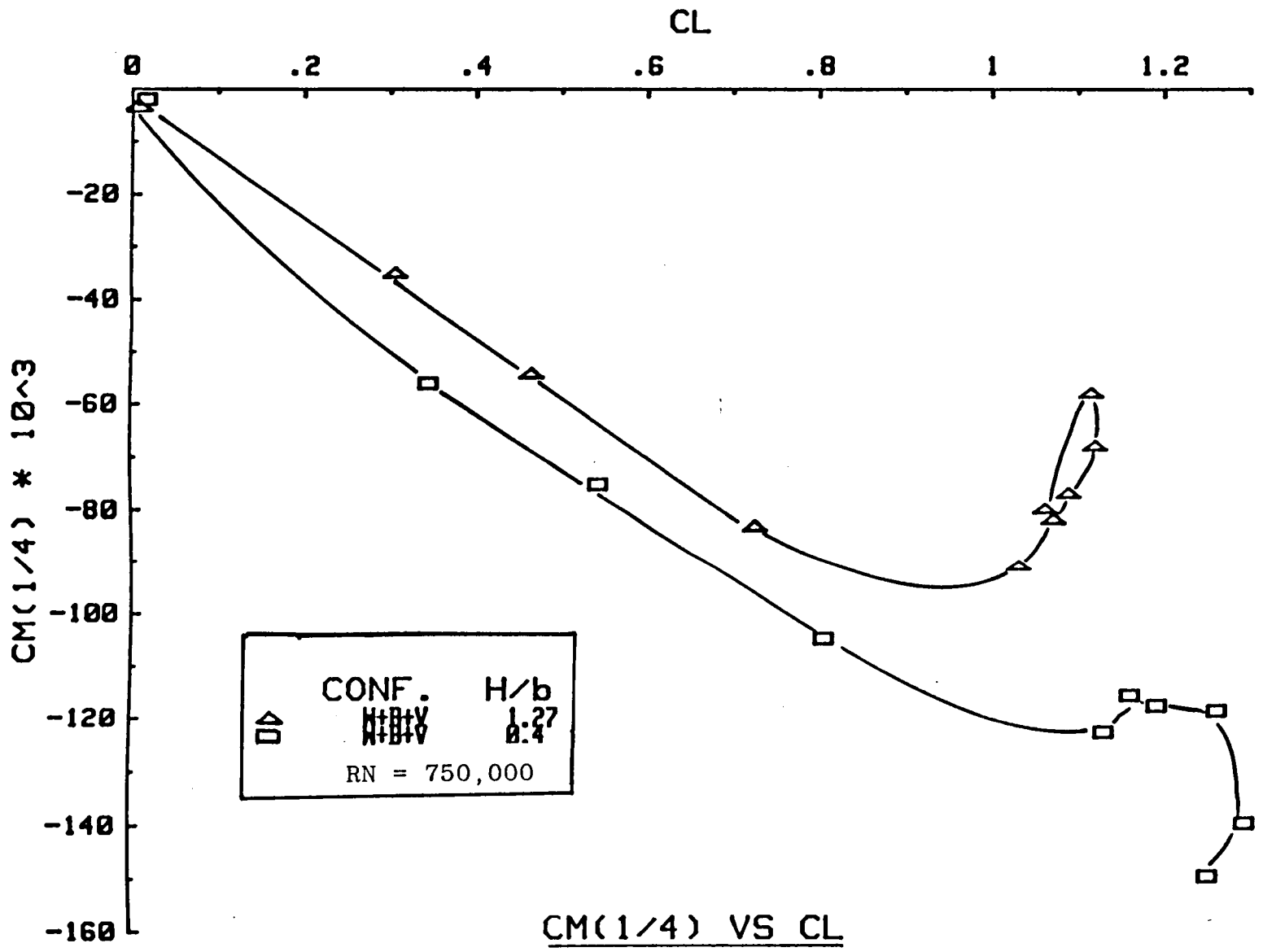

Figure 15C: Longitudinal Aerodynamic Characteristics for an XB-70-1 Model (W + B + V) in Static Ground Effect

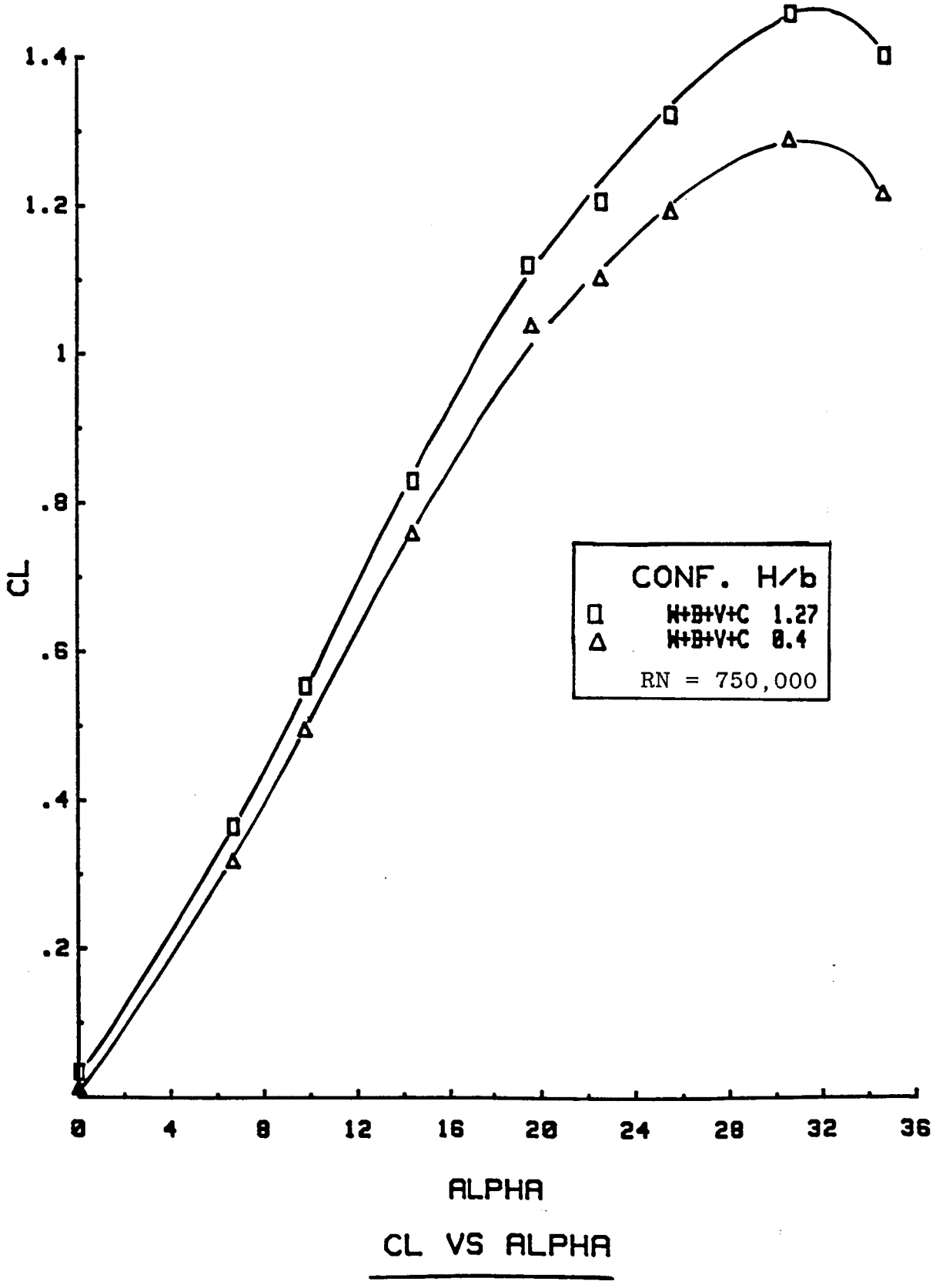

Figure 16A: Longitudinal Aerodynamic Characteristics for an XB-70-1 Model (W + B + V + C) in Static Ground Effect

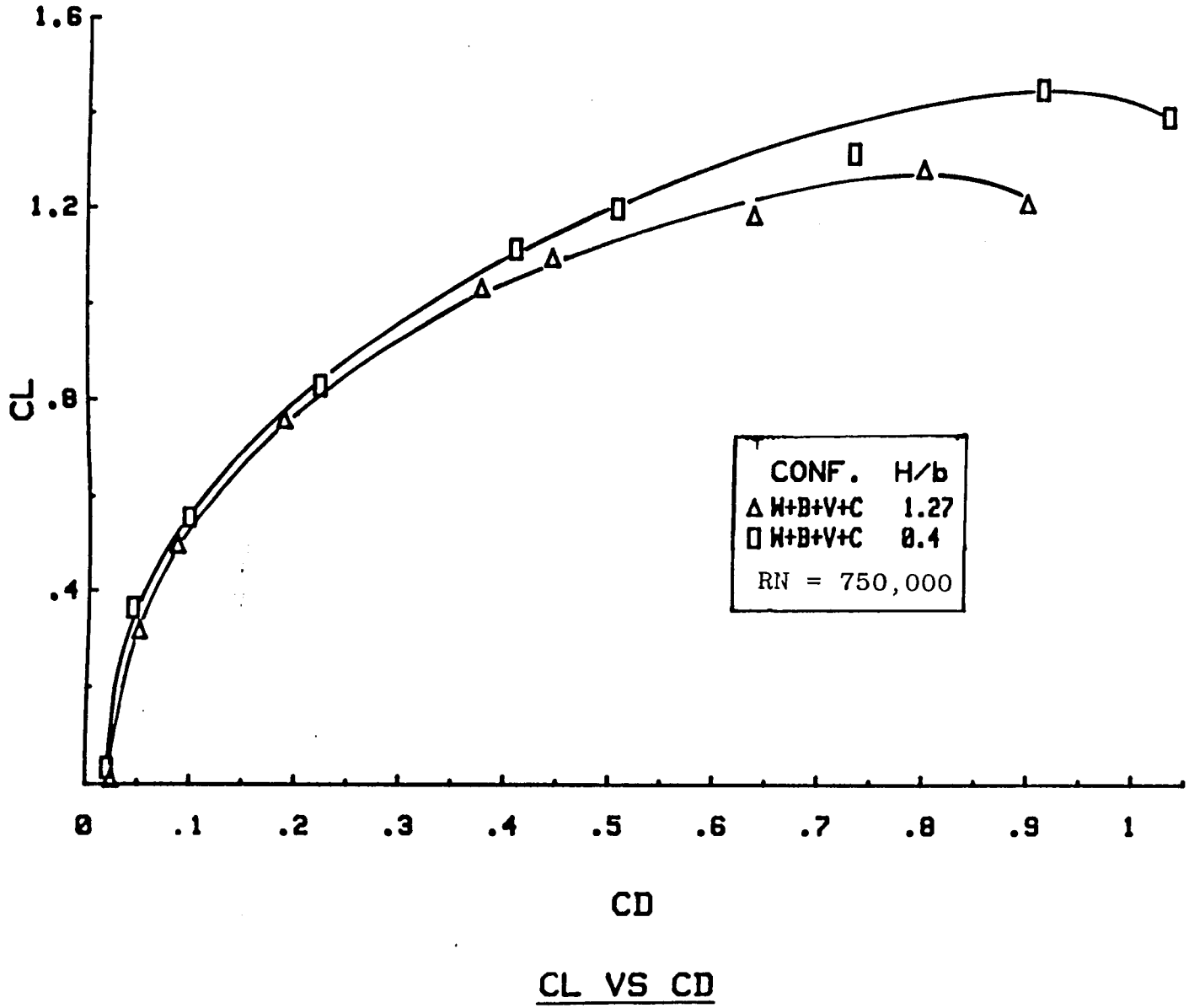

Figure 16B: Longitudinal Aerodynamic Characteristics for an XB-70-1 Model (W + B + V + C) in Static Ground Effect

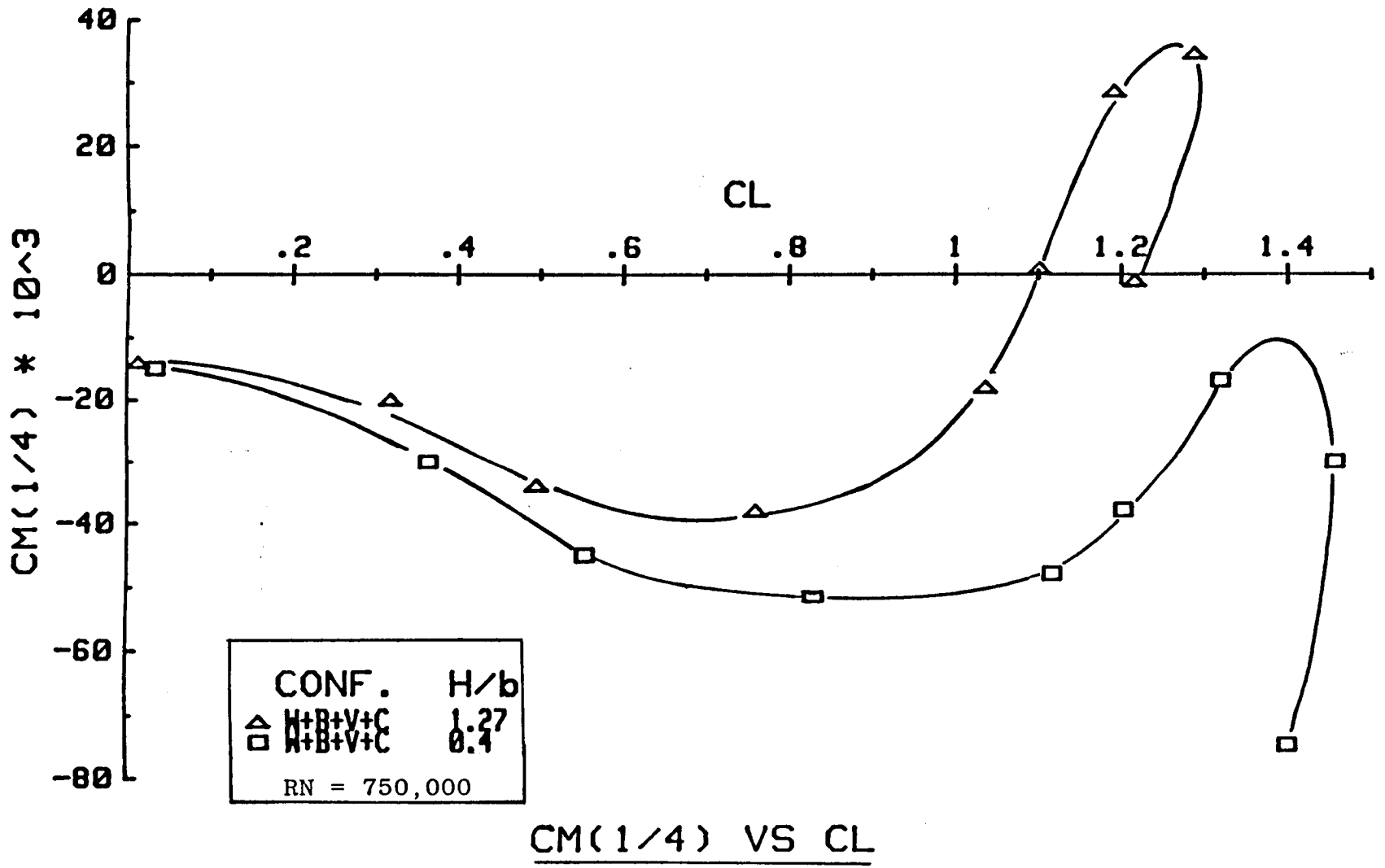

Figure 16C: Longitudinal Aerodynamic Characteristics for an XB-70-1 Model (W + B + V + C) in Static Ground Effect

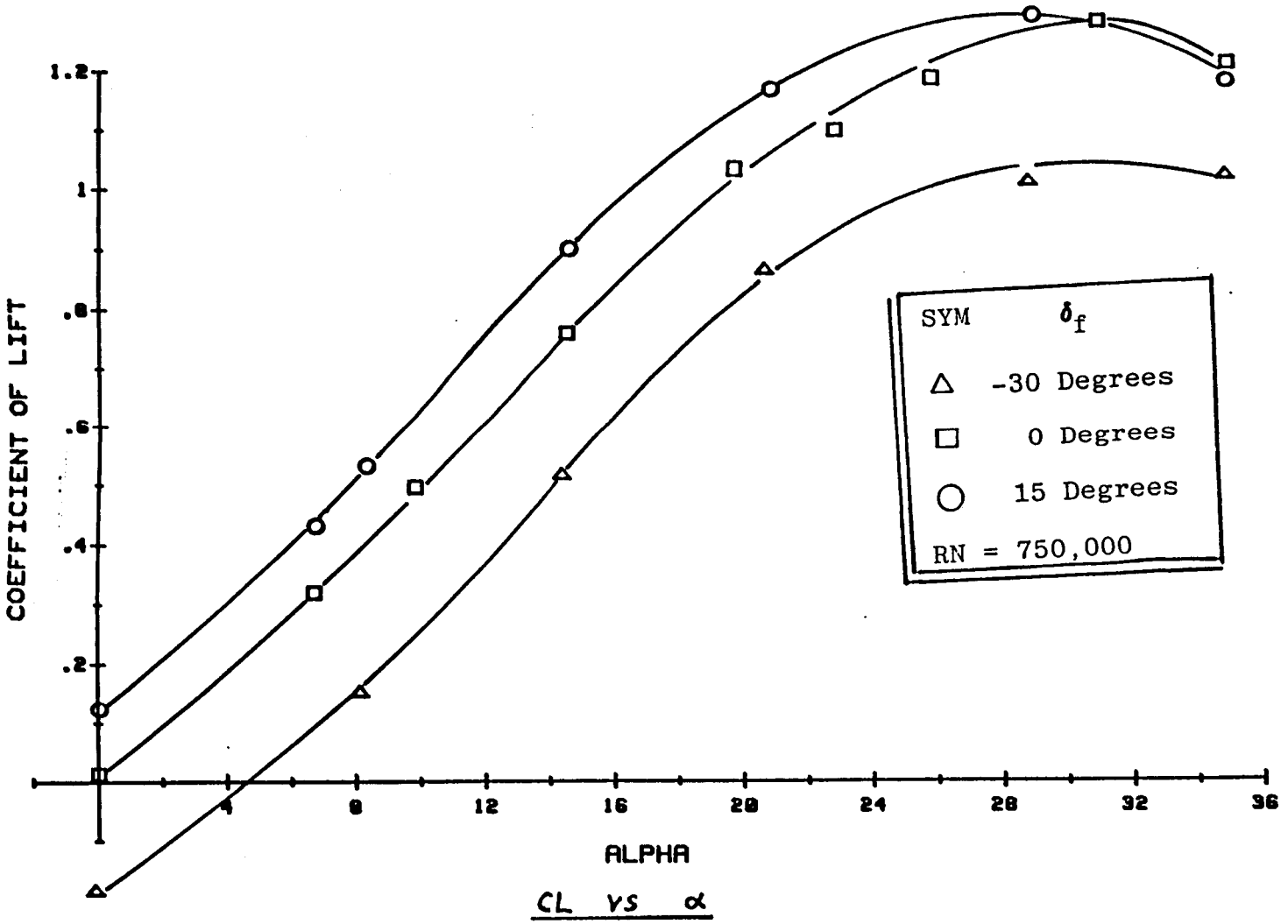

Figure 17A: Longitudinal Aerodynamic Characteristics for an XB-70-1 Model (W + B + V + C) with Flap Deflections in Out-of-Ground Effect

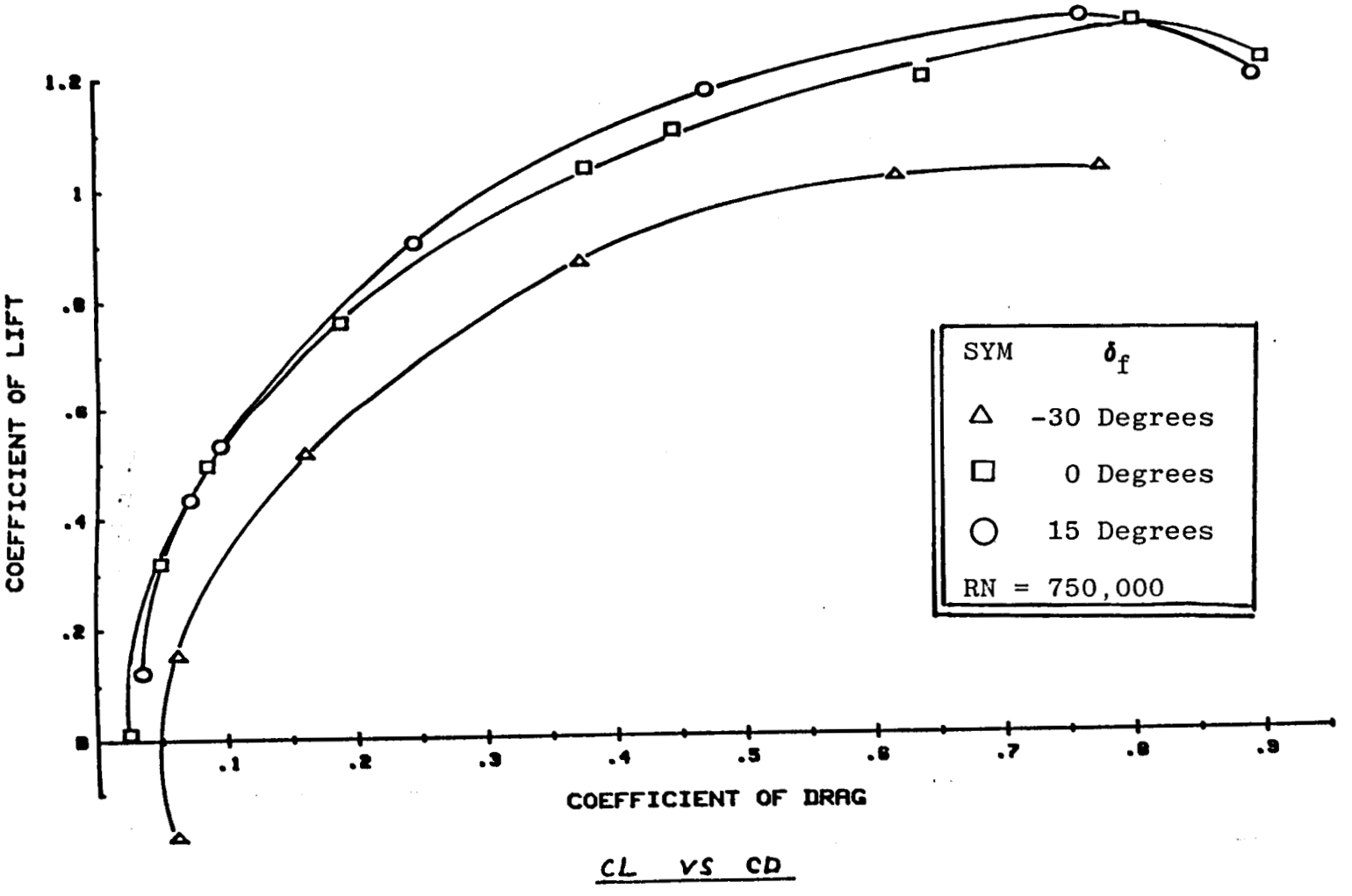

Figure 17B: Longitudinal Aerodynamic Characteristics for an XB-70-1 Model (W + B + V + C) with Flap Deflections in Out-of-Ground Effect

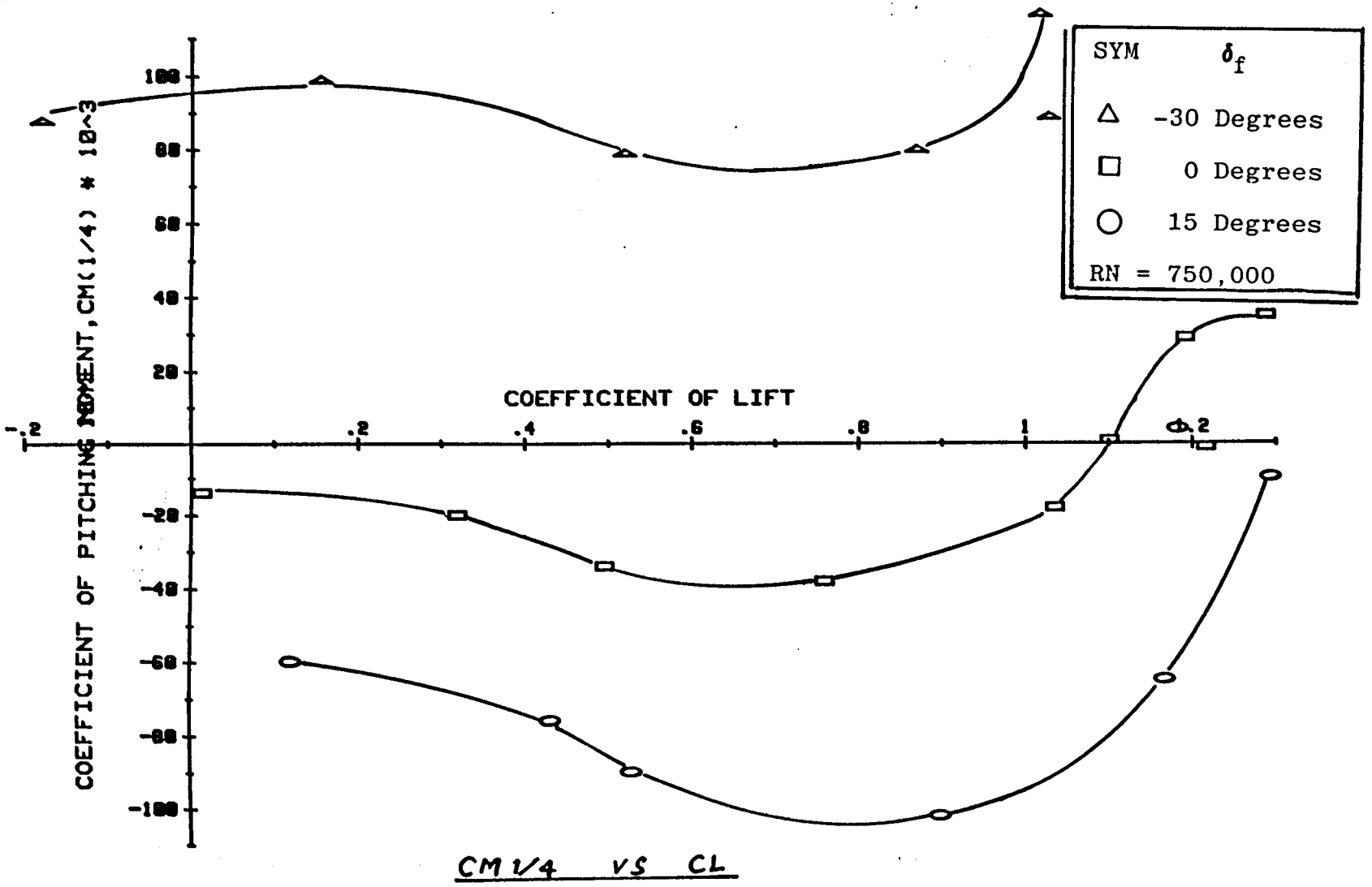

Figure 17C: Longitudinal Aerodynamic Characteristics for an XB-70-1 Model (W + B + V + C) with Flap Deflections in Out-of-Ground Effect

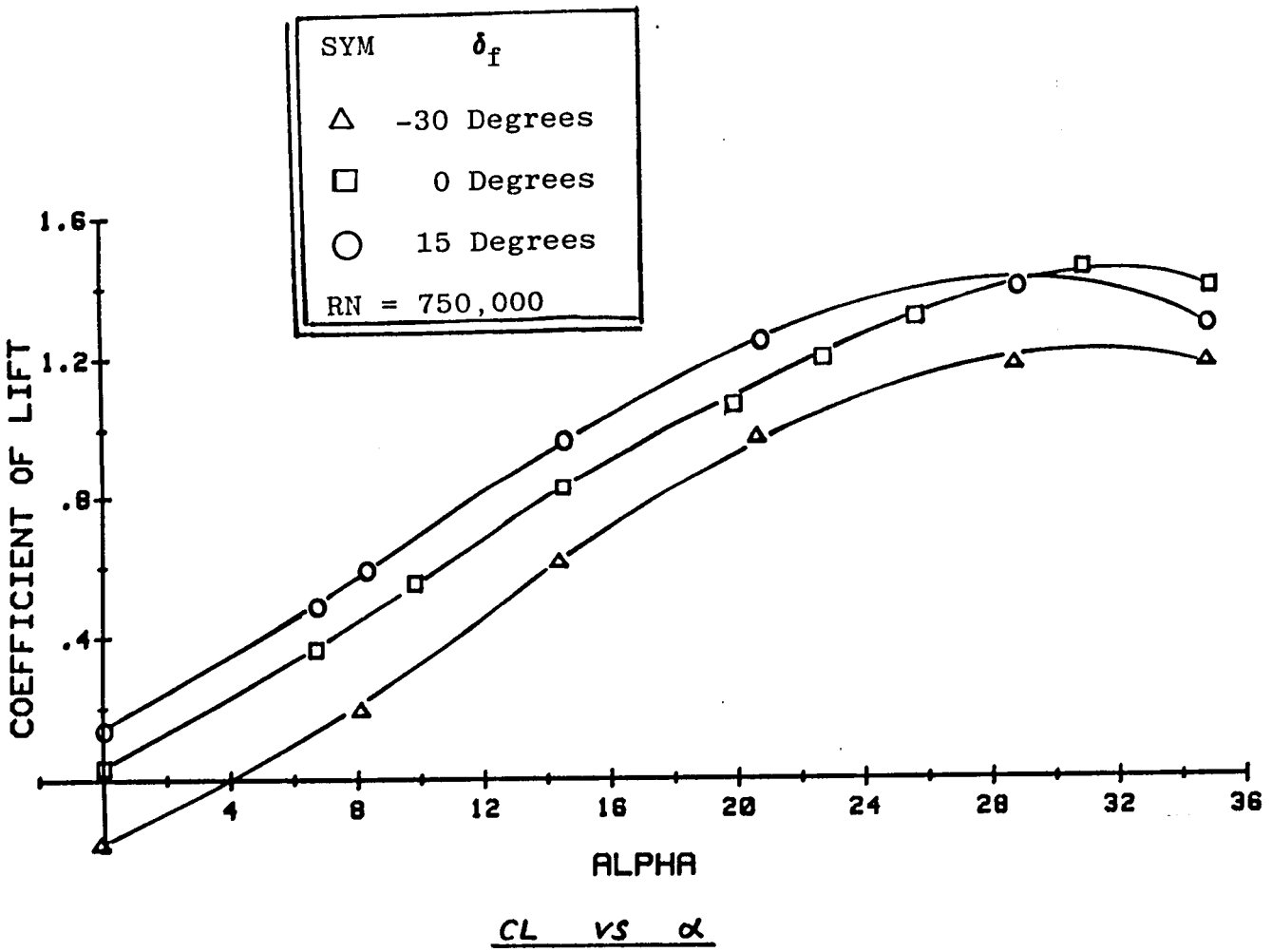

Figure 18A: Longitudinal Aerodynamic Characteristics for an XB-70-1 Model (W + B + V + C) with Flap Deflections in Static Ground Effect. H/b = 0.4.

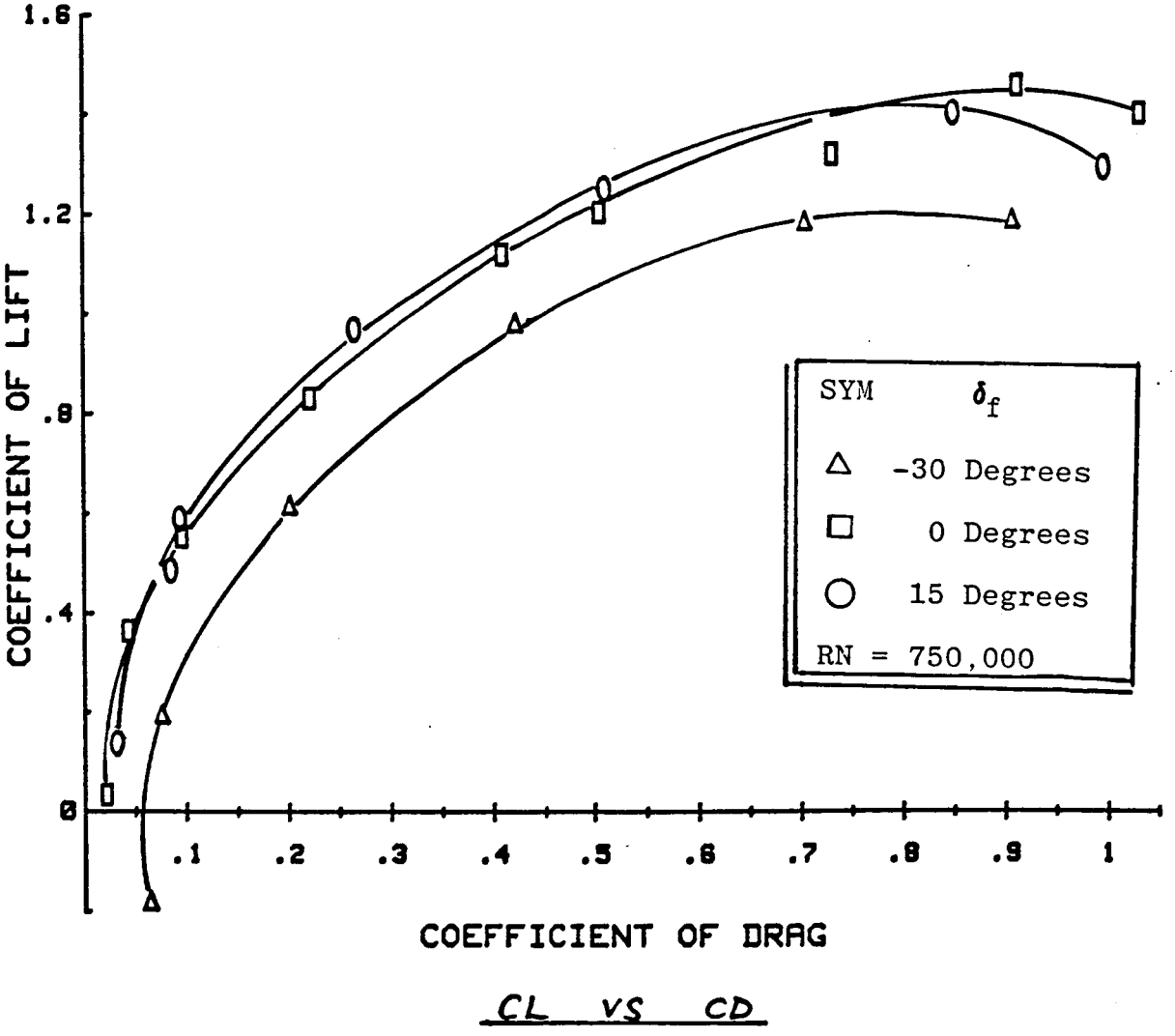

Figure 18B: Longitudinal Aerodynamic Characteristics for an XB-70-1 Model (W + B + V + C) with Flap Deflections in Static Ground Effect. H/b = 0.4.

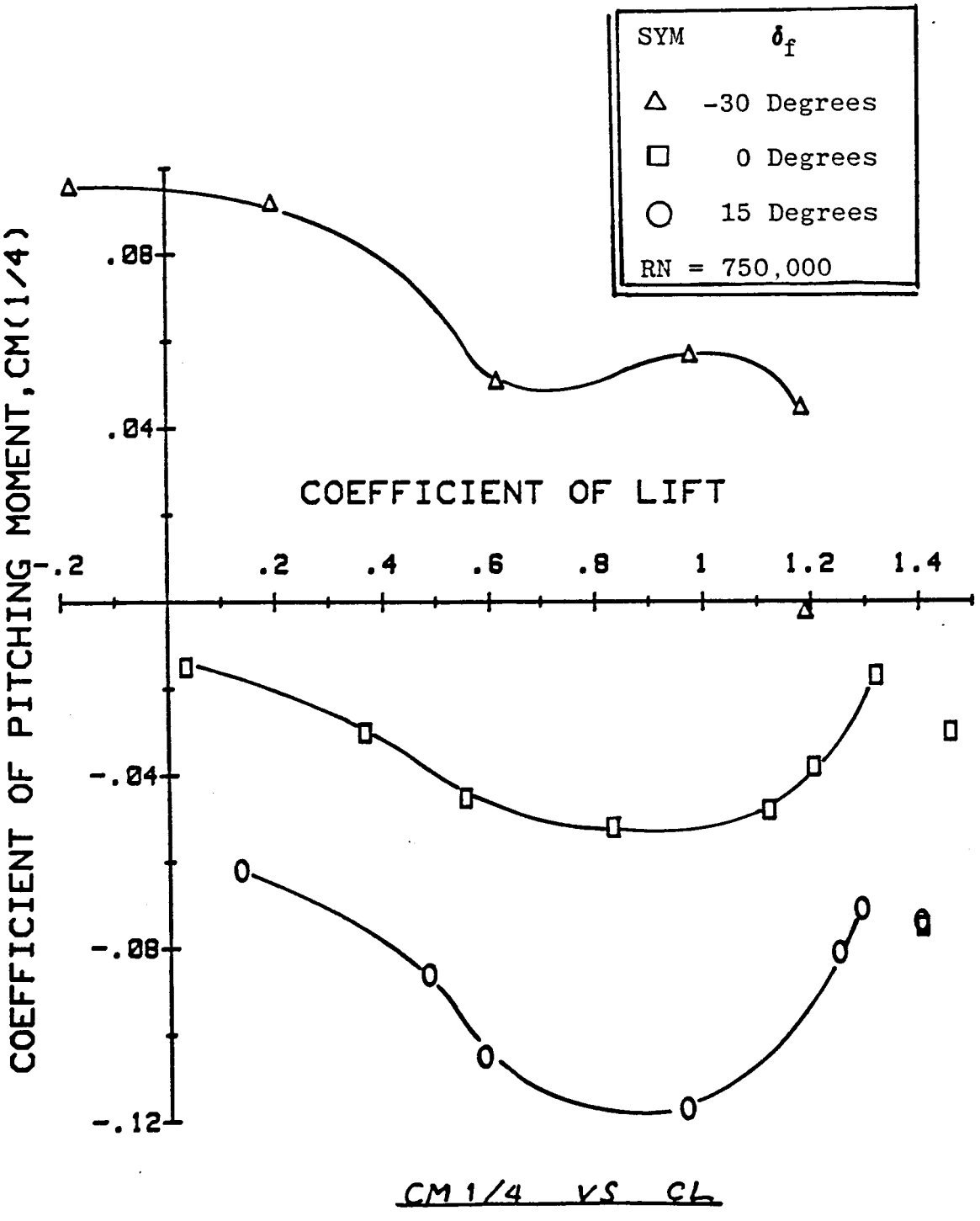

Figure 18C: Longitudinal Aerodynamic Characteristics for an XB-70-1 Model (W + B + V + C) with Flap Deflections in Static Ground Effect. H/b = 0.4.

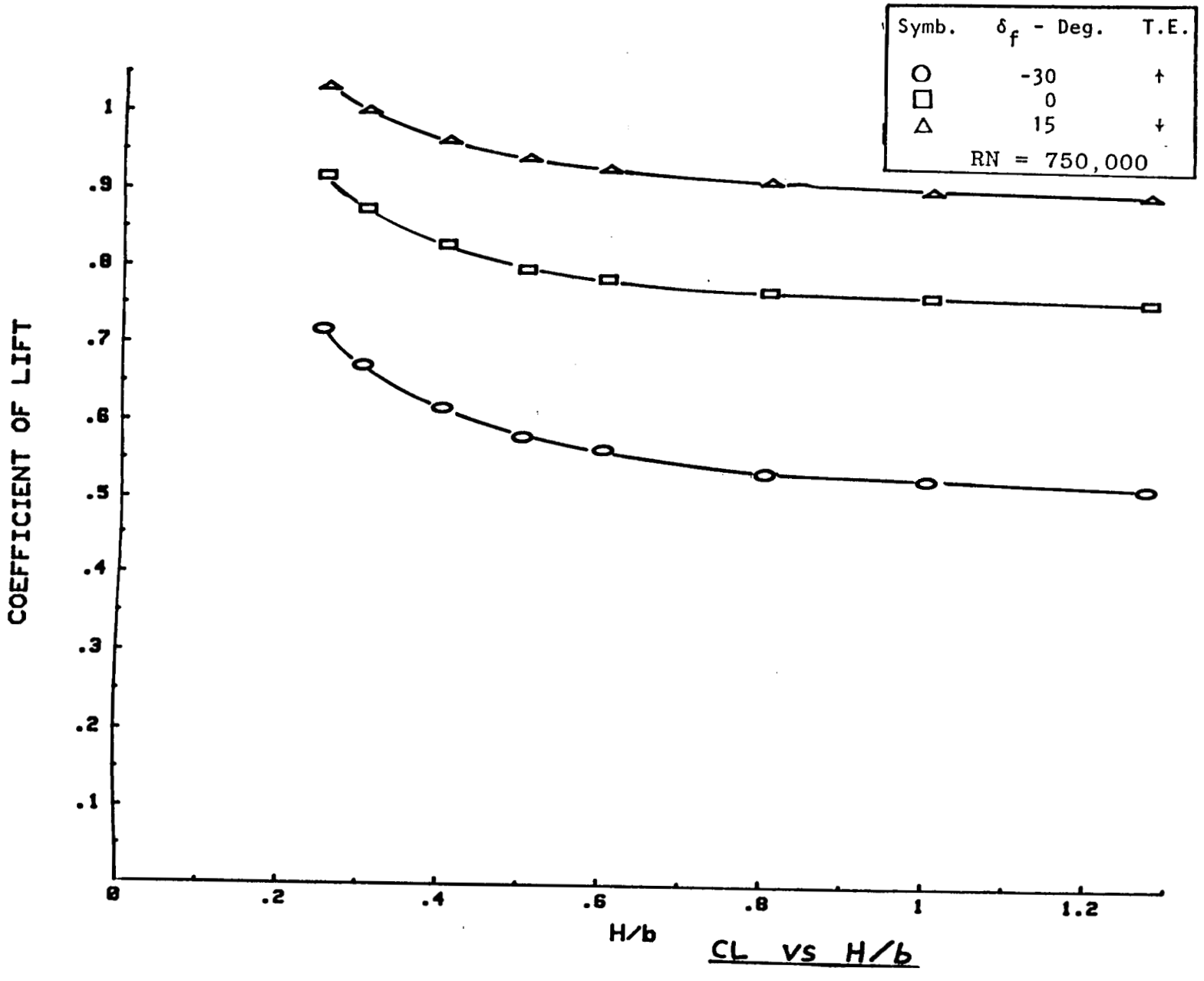

Figure 19A: Effect of Flap Deflections on Longitudinal Aerodynamic Characteristics for an XB-70-1 Model at α = 14 Degrees

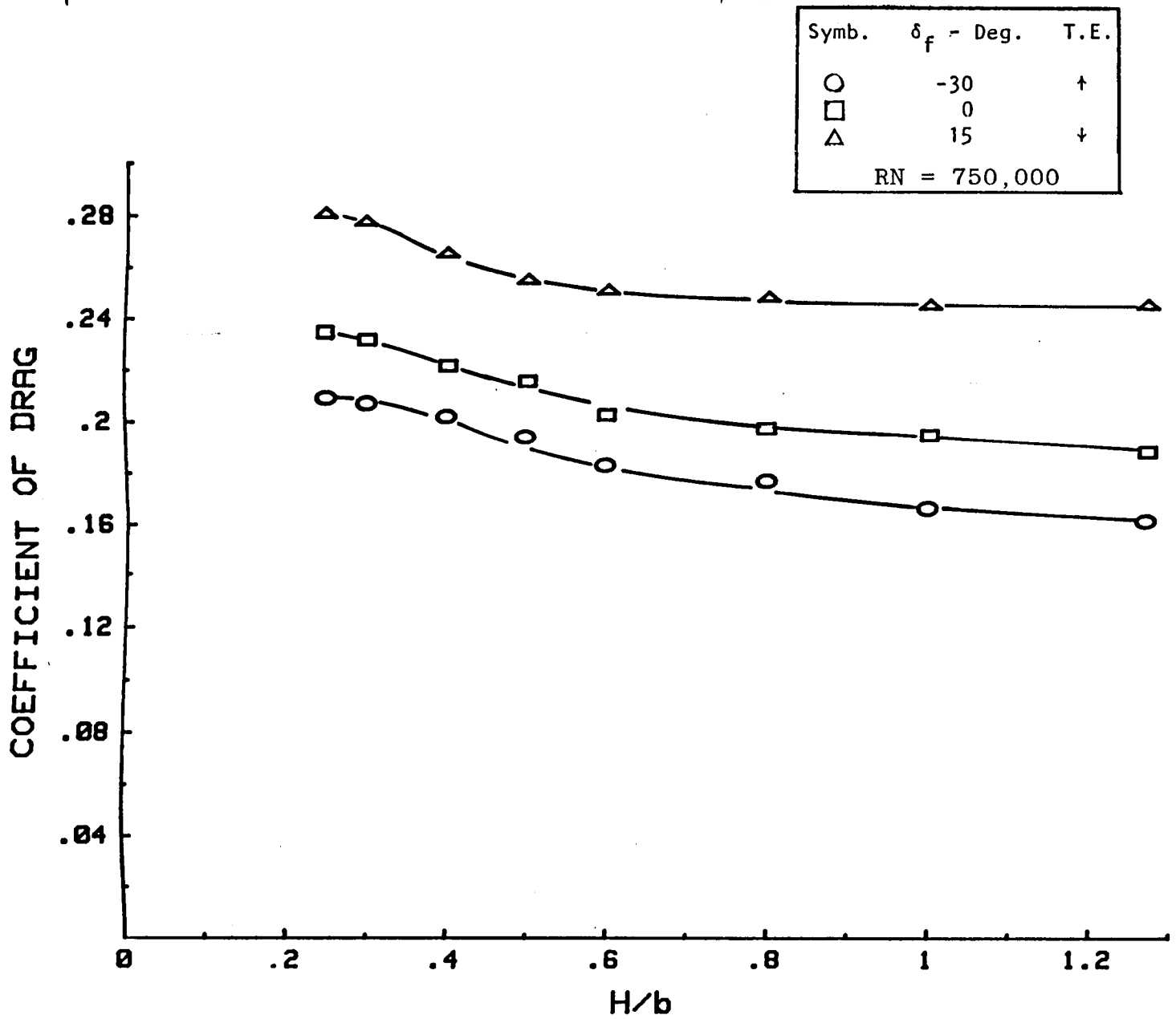

Figure 19B: Effect of Flap Deflections on Longitudinal Aerodynamic Characteristics for an XB-70-1 Model at α = 14 Degrees

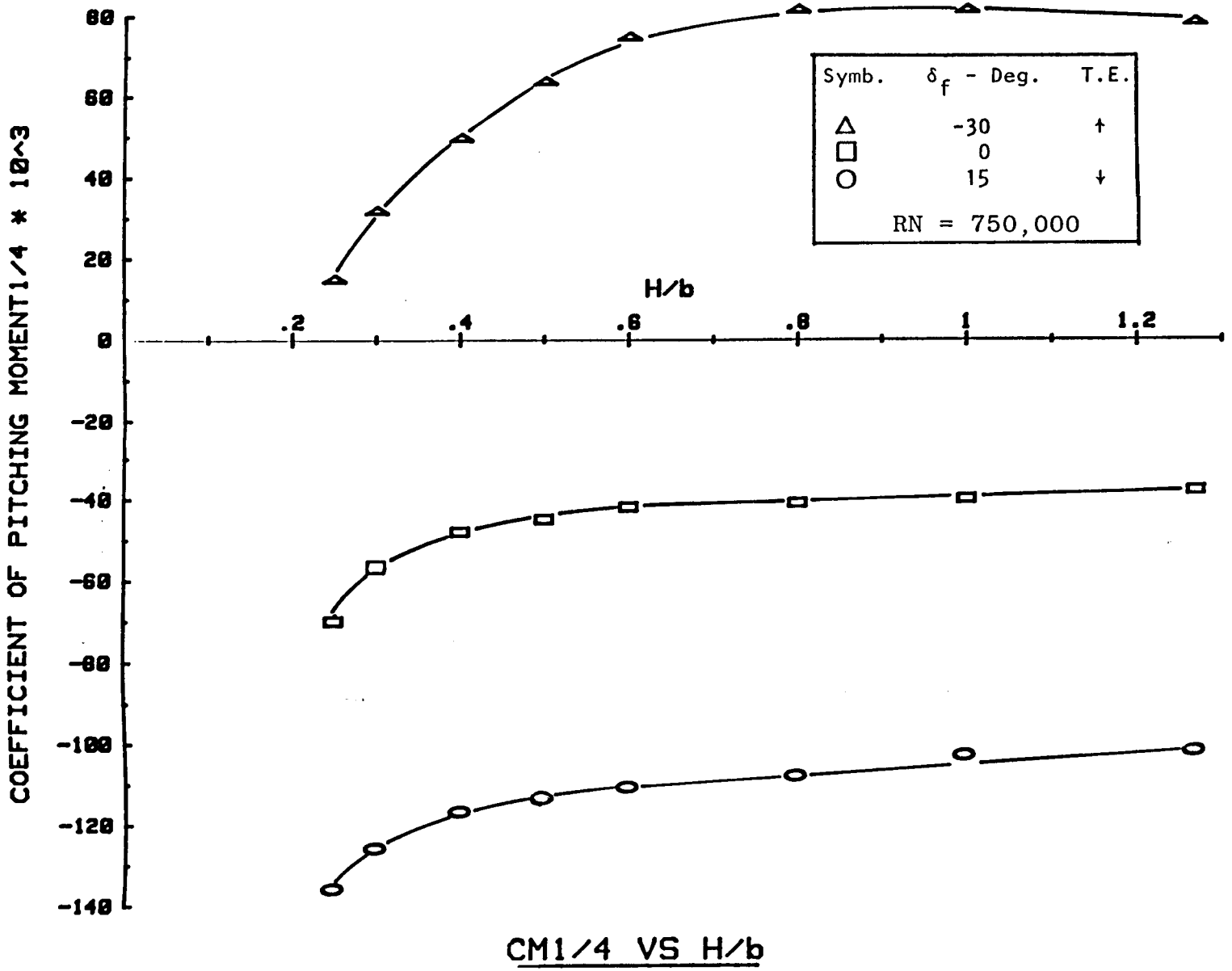

Figure 19C: Effect of Flap Deflections on Longitudinal Aerodynamic Characteristics for an XB-70-1 Model at α = 14 Degrees

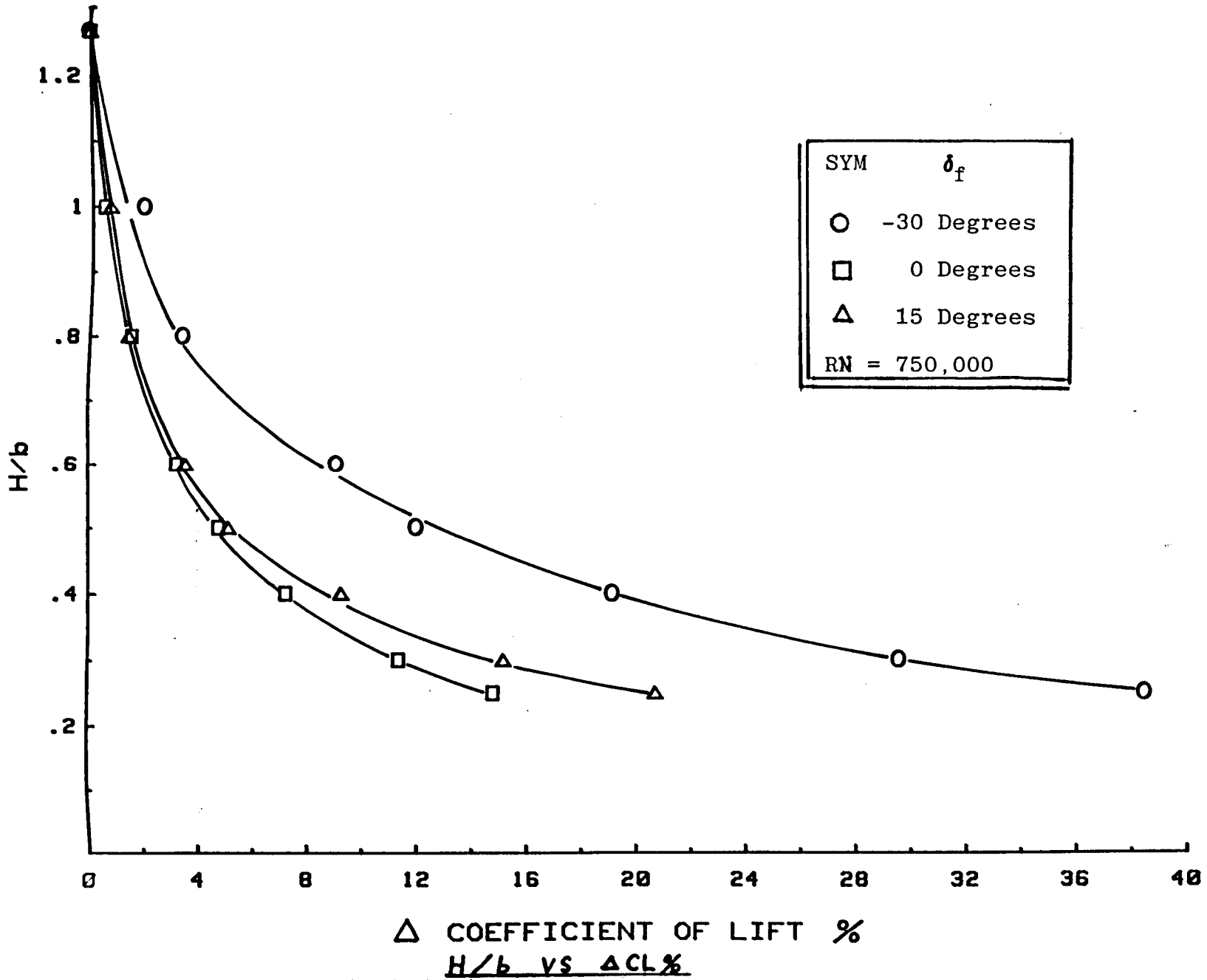

Figure 20A: Incremental Lift and Drag for an XB-70-1 Model with Flap Deflections in Static Ground Effect at α = 14 Degrees

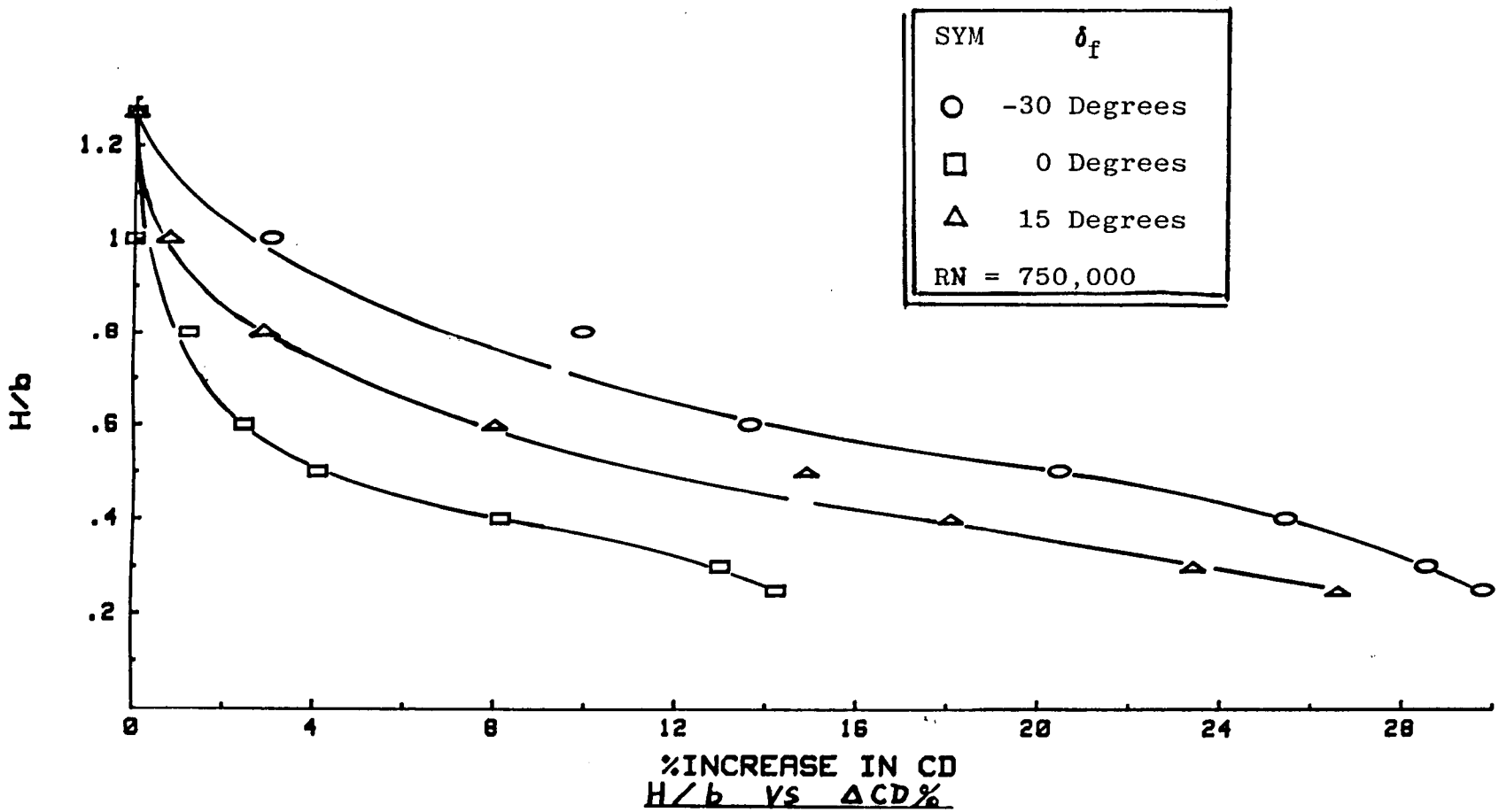

Figure 20B: Incremental Lift and Drag for an XB-70-1 Model with Flap Deflections in Static Ground Effect at α = 14 Degrees

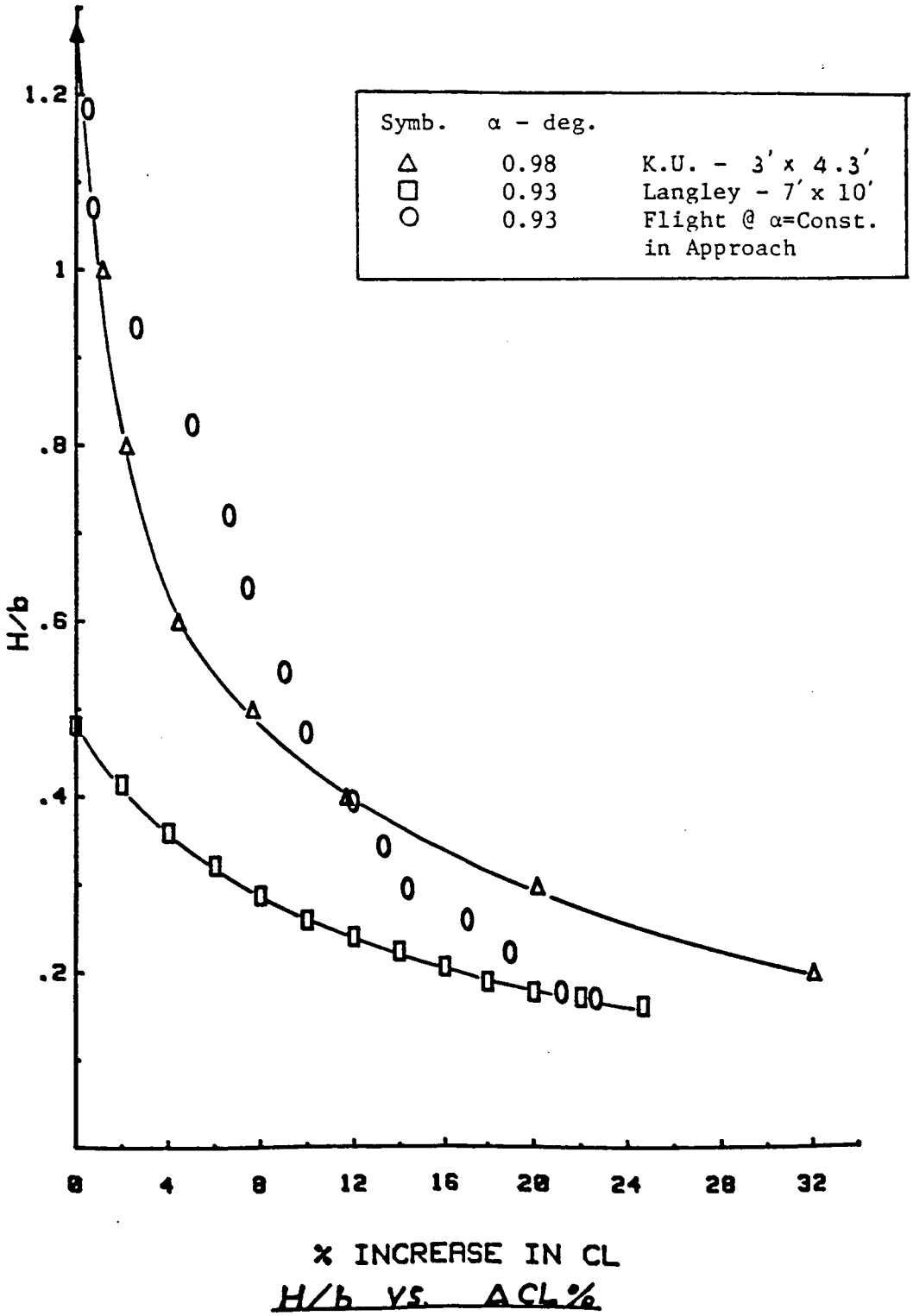

Figure 21: Comparison of Ground Effect Data for the XB-70-1 Configuration from Flight Test and Wind-Tunnel Static Test at α ≈ 9.5 Degrees